

American University in Cairo

## AUC Knowledge Fountain

---

Theses and Dissertations

Student Research

---

Winter 1-10-2022

# Multi-objective Optimization on Dimensional Accuracy, Edge and Surface Quality of 3D-Printed Parts by Fused Deposition Modelling

Islam Hamdy Salem

*The American University in Cairo AUC*, [ihamdys@aucegypt.edu](mailto:ihamdys@aucegypt.edu)

Follow this and additional works at: <https://fount.aucegypt.edu/etds>



Part of the [Manufacturing Commons](#)

---

### Recommended Citation

#### APA Citation

Salem, I. H. (2022). *Multi-objective Optimization on Dimensional Accuracy, Edge and Surface Quality of 3D-Printed Parts by Fused Deposition Modelling* [Master's Thesis, the American University in Cairo]. AUC Knowledge Fountain.

<https://fount.aucegypt.edu/etds/1881>

#### MLA Citation

Salem, Islam Hamdy. *Multi-objective Optimization on Dimensional Accuracy, Edge and Surface Quality of 3D-Printed Parts by Fused Deposition Modelling*. 2022. American University in Cairo, Master's Thesis. *AUC Knowledge Fountain*.

<https://fount.aucegypt.edu/etds/1881>

This Master's Thesis is brought to you for free and open access by the Student Research at AUC Knowledge Fountain. It has been accepted for inclusion in Theses and Dissertations by an authorized administrator of AUC Knowledge Fountain. For more information, please contact [thesisadmin@aucegypt.edu](mailto:thesisadmin@aucegypt.edu).



THE AMERICAN UNIVERSITY IN CAIRO  
SCHOOL OF SCIENCES AND ENGINEERING

**Multi-objective Optimization on Dimensional Accuracy, Edge and  
Surface Quality of 3D-Printed Parts by Fused Deposition  
Modelling**

BY

**Islam Hamdy Salem**

A thesis submitted in partial fulfilment of the requirements for the degree of

**Master of Science in Mechanical Engineering**

Under the supervision of:

**Dr. Mohamed Fawzy Aly**

**Associate Professor, Department of Mechanical Engineering**

**The American University in Cairo**

**January 2022**

# DEDICATION

Special dedication to my beloved father Prof. Hamdy Salem who I wish he could witness these moments with me. This is your fruitful harvest. I pray to Allah to bliss your soul. I just miss you, and I hope you are proud of my dad.

Also, dedicated to my beloved family, mom, brother and my future beloved wife, who never gave up on me and supported me until the end of the journey.

# ACKNOWLEDGMENT

Words cannot describe my gratitude to my supervisor Dr. Mohamed Fawzy Aly. Many thanks for his support and guidance. Much more thanks for his patience and appreciation through the obstacles I faced during my degree journey. Not only did he treat me as my supervisor, but he also was a supportive elder brother.

I also would like to acknowledge Dr. Khalil El-Khodary for the precious knowledge he transferred to me during my degree courses I have attended with him. I am very grateful for the fruitful outcomes I gain from him.

Also, I would like to thank Dr. Ahmed El-Kaseer for his priceless advice to save the last breaths of my degree journey. He was very generous and helpful to me.

Special thanks to the Pixel Lab company technical support team who did not hesitate to support my experimental work and never let me down.

Finally, I would like to thank all AUC members who supported me during my degree. Special thanks to AUC graduate office for their research funding that I would not have done this research without.

## ABSTRACT

Fused Deposition Modelling (FDM) is one of most common additive manufacturing (AM) techniques used in manufacturing field. It has been increasingly used because of its low cost and simplicity. Although FDM can save time through eliminating pre-processing tooling-up to produce the end-user product, still a better final product quality, like mechanical properties, dimensional accuracy and surface finish, is needed. This thesis addresses the maximization of involved printing parameters in one reliable model. Hence, a wider investigation is conducted in this research via experimental work in order to obtain a comprehensive model that involves and relates more parameters in a single model. A full factorial 2-level DOE is used for 6 printing parameters; layer height, wall thickness, bottom/top thickness, infill density, temperature and printing speed. The results of experiment were analyzed using ANOVA analysis, and the regression models were developed. The regression models showed some weakness in the goodness of fit due to the large number of hidden variables and uncertainty of the FDM process. Layer height, wall thickness, infill density, printing speed and their interactions were found to be the most influential on the dimensional accuracy, edge quality and surface quality. Finally, the obtained regression models were optimized by two different multi-objective optimization techniques, and the optimal printing parameters were identified and tested.

# TABLE OF CONTENTS

Dedication .....	i
Acknowledgment .....	ii
Abstract .....	iii
Table of Contents .....	iv
List of Tables .....	vi
List of Figures .....	vii
List of Symbols .....	xi
List of Abbreviations .....	xii
Chapter One: Introduction .....	1
1.1. Background .....	1
1.2. Problem Statement .....	3
1.3. Thesis Objectives .....	4
1.4. Thesis Layout .....	4
Chapter Two: Literature Review .....	6
Research Aims.....	11
Chapter Three: Experimental Work.....	12
3.1. Equipment Setup and Material.....	12
3.2. Design of Experiment (DOE).....	14
3.3. Parameters and Slicing .....	16
3.4. Measurements and Measurement Tool .....	17
Chapter Four: Results and Discussions.....	22
4.1. Results of Cube Samples.....	22
4.2. Results of Cylinder Samples .....	22
4.3. Analysis of Variance (ANOVA).....	23
4.3.1. Cube Model Analysis.....	23
4.3.2. Cylinder Model Analysis .....	36
4.4. Multi-Objective Optimization .....	47
4.5. Discussion .....	52
Chapter Five: Conclusions and Future Work.....	55
5.1. Conclusions .....	55
5.2. Future Work .....	56
References.....	57

Appendix.....	60
A.    Experimental Results of Cube Samples .....	60
B.    Experimental Results of Cylinder Samples.....	62

# LIST OF TABLES

Table 1: Physical and mechanical properties of (PLA+).	12
Table 2: Table of parameters and levels.	15
Table 3: Fixed running conditions.	16
Table 4: ANOVA table of dimensional variation of cube samples.	26
Table 5: ANOVA table of edge quality of cube samples.	30
Table 6: ANOVA table of surface quality of cube samples.	33
Table 7: ANOVA table of dimensional variation of cylinder samples.	38
Table 8: ANOVA table of edge quality of cylinder samples.	41
Table 9: ANOVA table of surface quality of cylinder samples.	44
Table 10: Optimization model of cube samples.	47
Table 11: MOGA optimal solution for cube samples.	48
Table 12: MOPSA optimal solution for cube samples.	49
Table 13: Optimization model of cylinder samples.	50
Table 14: MOGA optimal solution for cylinder samples.	51
Table 15: MOPSA optimal solution for cylinder samples.	51
Table 16: Comparison between different optimization techniques on cube and cylinder cases. .....	54
Table 17: Comparison between printed samples with optimal parameters and the obtained model.....	54



# LIST OF FIGURES

Figure 1: FDM process schematic [8].	2
Figure 2: Stair case effect on surface quality [15].	3
Figure 3: (a) Print orientation of cylinder parts, and (b) parameters used to print dog bone samples [34].	9
Figure 4: (a) CAD model of test sample including various geometries, and (b) final printed samples [35].	10
Figure 5: Brown color PLA+ filament of 1.75mm diameter.	12
Figure 6: MakerX Pro 3D printer details.	14
Figure 7: Ultimaker Cura slicing preview mode (Copyrights reserved to Ultimaker company).	17
Figure 8: Measured cube dimensions.	18
Figure 9: Measured cylinder dimensions.	19
Figure 10: INSIZE digital caliper "Code 1108-150".	19
Figure 11: Printing parts edge defects.	20
Figure 12: Printing parts surface defects.	21
Figure 13: Main effects plot for dimensional variation of cube samples.	24
Figure 14: Main effects plot for edge quality for cube samples.	25
Figure 15: Main effects plot for surface quality for cube samples.	25
Figure 16: Normal probability plot of residuals for the dimensional variation regression of cube samples.	27

Figure 17: Histogram of residuals for the dimensional variation regression of cube samples. .....	28
Figure 18: Parameters' interactions of the dimensional variation regression of cube samples: (a) <i>LH</i> and <i>Wt</i> , (b) <i>LH</i> and <i>BTt</i> , (c) <i>LH</i> and <i>InD</i> , (d) <i>LH</i> and <i>T</i> , (e) <i>LH</i> and <i>V</i> , (f) <i>Wt</i> and <i>BTt</i> , (g) <i>Wt</i> and <i>InD</i> , (h) <i>Wt</i> and <i>T</i> , (i) <i>Wt</i> and <i>V</i> , (j) <i>BTt</i> and <i>InD</i> , (k) <i>BTt</i> and <i>T</i> , (l) <i>BTt</i> and <i>V</i> , (m) <i>InD</i> and <i>T</i> , (n) <i>InD</i> and <i>V</i> and (o) <i>T</i> and <i>V</i> . ....	29
Figure 19: Normal probability plot of residuals for the edge quality regression of cube samples. .....	31
Figure 20: Histogram of residuals for the edge quality regression of cube samples. ....	31
Figure 21: Parameters' interactions of the edge quality regression of cube samples: (a) <i>LH</i> and <i>Wt</i> , (b) <i>LH</i> and <i>BTt</i> , (c) <i>LH</i> and <i>InD</i> , (d) <i>LH</i> and <i>T</i> , (e) <i>LH</i> and <i>V</i> , (f) <i>Wt</i> and <i>BTt</i> , (g) <i>Wt</i> and <i>InD</i> , (h) <i>Wt</i> and <i>T</i> , (i) <i>Wt</i> and <i>V</i> , (j) <i>BTt</i> and <i>InD</i> , (k) <i>BTt</i> and <i>T</i> , (l) <i>BTt</i> and <i>V</i> , (m) <i>InD</i> and <i>T</i> , (n) <i>InD</i> and <i>V</i> and (o) <i>T</i> and <i>V</i> .....	32
Figure 22: Normal probability plot of residuals for the surface quality regression of cube samples.....	34
Figure 23: Histogram of residuals for the surface quality regression of cube samples. ....	34
Figure 24: Parameters' interactions of the surface quality regression of cube samples: (a) <i>LH</i> and <i>Wt</i> , (b) <i>LH</i> and <i>BTt</i> , (c) <i>LH</i> and <i>InD</i> , (d) <i>LH</i> and <i>T</i> , (e) <i>LH</i> and <i>V</i> , (f) <i>Wt</i> and <i>BTt</i> , (g) <i>Wt</i> and <i>InD</i> , (h) <i>Wt</i> and <i>T</i> , (i) <i>Wt</i> and <i>V</i> , (j) <i>BTt</i> and <i>InD</i> , (k) <i>BTt</i> and <i>T</i> , (l) <i>BTt</i> and <i>V</i> , (m) <i>InD</i> and <i>T</i> , (n) <i>InD</i> and <i>V</i> and (o) <i>T</i> and <i>V</i> . ....	35
Figure 25: Main effects plot for dimensional variation of cylinder samples. ....	36
Figure 26: Main effects plot for edge quality of cylinder samples. ....	37
Figure 27: Main effects plot for surface quality of cylinder samples. ....	37

Figure 28: Normal probability plot of residuals for the dimensional variation regression of cylinder samples.....	39
Figure 29: Histogram of residuals for the dimensional variation regression of cylinder samples. .....	39
Figure 30: Parameters' interactions of the dimensional variation regression of cylinder samples: (a) <i>LH</i> and <i>Wt</i> , (b) <i>LH</i> and <i>BTt</i> , (c) <i>LH</i> and <i>InD</i> , (d) <i>LH</i> and <i>T</i> , (e) <i>LH</i> and <i>V</i> , (f) <i>Wt</i> and <i>BTt</i> , (g) <i>Wt</i> and <i>InD</i> , (h) <i>Wt</i> and <i>T</i> , (i) <i>Wt</i> and <i>V</i> , (j) <i>BTt</i> and <i>InD</i> , (k) <i>BTt</i> and <i>T</i> , (l) <i>BTt</i> and <i>V</i> , (m) <i>InD</i> and <i>T</i> , (n) <i>InD</i> and <i>V</i> and (o) <i>T</i> and <i>V</i> . ....	40
Figure 31: Normal probability plot of residuals for the edge quality regression of cylinder samples.....	42
Figure 32: Histogram of residuals for the edge quality regression of cylinder samples.....	42
Figure 33: Parameters' interactions of the edge quality regression of cylinder samples: (a) <i>LH</i> and <i>Wt</i> , (b) <i>LH</i> and <i>BTt</i> , (c) <i>LH</i> and <i>InD</i> , (d) <i>LH</i> and <i>T</i> , (e) <i>LH</i> and <i>V</i> , (f) <i>Wt</i> and <i>BTt</i> , (g) <i>Wt</i> and <i>InD</i> , (h) <i>Wt</i> and <i>T</i> , (i) <i>Wt</i> and <i>V</i> , (j) <i>BTt</i> and <i>InD</i> , (k) <i>BTt</i> and <i>T</i> , (l) <i>BTt</i> and <i>V</i> , (m) <i>InD</i> and <i>T</i> , (n) <i>InD</i> and <i>V</i> and (o) <i>T</i> and <i>V</i> . ....	43
Figure 34: Normal probability plot of residuals for the surface quality regression of cylinder samples.....	45
Figure 35: Histogram of residuals for the surface quality regression of cylinder samples.....	45
Figure 36: Parameters' interactions of the surface quality regression of cylinder samples: (a) <i>LH</i> and <i>Wt</i> , (b) <i>LH</i> and <i>BTt</i> , (c) <i>LH</i> and <i>InD</i> , (d) <i>LH</i> and <i>T</i> , (e) <i>LH</i> and <i>V</i> , (f) <i>Wt</i> and <i>BTt</i> , (g) <i>Wt</i> and <i>InD</i> , (h) <i>Wt</i> and <i>T</i> , (i) <i>Wt</i> and <i>V</i> , (j) <i>BTt</i> and <i>InD</i> , (k) <i>BTt</i> and <i>T</i> , (l) <i>BTt</i> and <i>V</i> , (m) <i>InD</i> and <i>T</i> , (n) <i>InD</i> and <i>V</i> and (o) <i>T</i> and <i>V</i> .....	46
Figure 37: Parallel Plot of MOGA simulation for cube samples.....	48
Figure 38: Parallel Plot of MOPSA simulation for cube samples. ....	49

Figure 39: Parallel Plot of MOGA simulation for cylinder samples. ....50

Figure 40: Parallel Plot of MOPSA simulation for cylinder samples.....51

Figure 41: Printed samples using the optimal parameters obtained in the study.....53

# LIST OF SYMBOLS

Symbol	Definition
<i>LH</i>	Layer Height (mm)
<i>Wt</i>	Wall thickness (mm)
<i>BTt</i>	Bottom/top thickness (mm)
<i>InD</i>	Infill Density (%)
<i>T</i>	Temperature (°C)
<i>V</i>	Printing speed (mm/s)
Subscript <i>n</i>	Normalized parameter [-1 1]
<i>DV</i>	Dimensional variation

## LIST OF ABBREVIATIONS

Abbreviation	Definition
ABS	Acrylonitrile-Butadiene-Styrene
AM	Additive Manufacturing
ANOVA	Analysis of Variance
CAD	Computer-Aided Design
FDM	Fused Deposition Modeling
FEA	Finite Element Analysis
FFF	Fused Filament Fabrication
IRP	Intelligent Rapid Prototyping
MOGA	Multi-Objective Genetic Algorithm
MOPSA	Multi-Objective Pareto Search Algorithm
NSGA II	Non-Dominated Sorting Genetic Algorithm II
PLA	Polylactic Acid
RP	Rapid Prototyping
SLA	Stereolithography
S/N	Signal to Noise ratio
STL	Standard Tessellation Language

# CHAPTER ONE: INTRODUCTION

## 1.1. Background

Additive Manufacturing (AM) is considered a new terminology for many researchers in the manufacturing field. Intuitively, the term additive can explain the new terminology. AM is the building of the final part from zero material until full complex geometries without the need for removing extra material nor pre-process tooling up. Also, AM is commonly known as 3D printing, which was first developed by Charles W. Hull in the mid-1980s. In detail, AM process sequence starts with a computer aided design (CAD) model by means of 3D-modelling software. Hence, the model is converted to a .STL file in which the 3D model is sliced into very thin layers. Thereafter, the file is exported to a 3D slicer software to translate the sliced layers to a toolpath, like a G-code file. Finally, the part is ready to be printed by adding the material layer-by-layer until the complete geometry is created [1], [2]. The various 3D printing techniques can be categorized into three types, which are solid-based, liquid-based, and powder-based [3], [4]. Amongst the various 3D printing processes, fused deposition modeling (FDM) or fused filament fabrication (FFF) is the most commonly used, which will be the focus in this research. The creation of FDM was introduced by S. Scott Crump in the late 1988s [5]. FDM material is preferred to be a thermoplastic filament as a printing material. The filament is passed through an extruder to a hot end with a heater inside to heat the material to a specific temperature. The material is extruded through a heated nozzle to a platform (build bed) where the part is printed and created [5]–[8]. The FDM process schematic is shown in Figure 1.

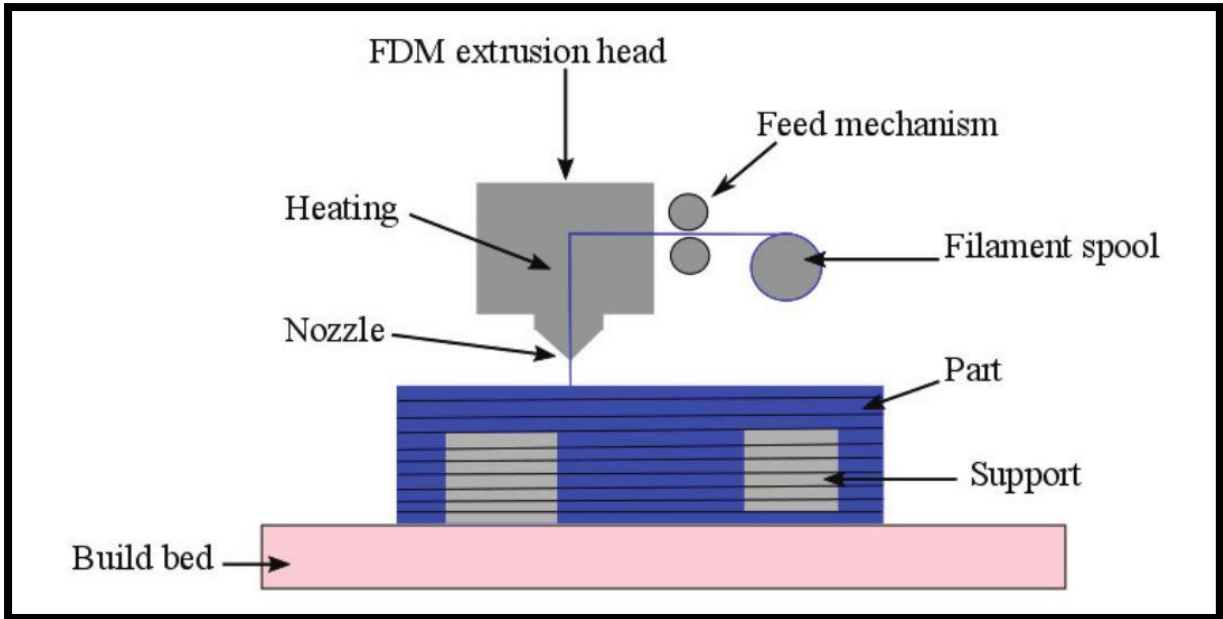


Figure 1: FDM process schematic [8].

The main advantages of AM are low cost as material wastes are almost zero, the availability of the core knowledge, the capability of creating complex and customized geometries in one step rather than conventional manufacturing processes [9], and the independence on pre-processing. These advantages place AM as the first choice when it comes to job-shop or batch production, which strengthens the AM against the competition with the conventional manufacturing processes [10]. Recently, AM has been used in many applications and fields like rapid prototyping RP, biomedical, building and construction, aerospace and protective structures [2], [3]. Notwithstanding, AM still challenges many limitations that prevent the full replacement of conventional processes by AM. The remarkable drawbacks of AM can be concluded in processing time, surface defects (see Figure 2), voids creation on top surface, layers delamination, geometrical errors on edges, weak mechanical strength due to the anisotropic behavior of the printed parts, the limited number of material used in 3D printing, design of 3D printing and slicing software, hardware and maintenance issues, part orientation which involves overcoming the problem of overhanging and toolpath and, finally, post-processing due to undesirable surface finish and inaccurate dimensions [3], [6], [7], [10]–[14].



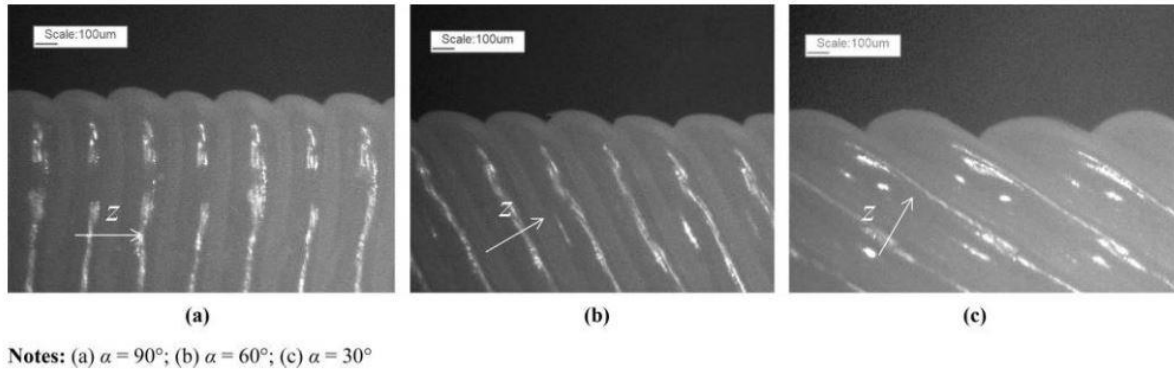


Figure 2: Stair case effect on surface quality [15].

One of the critical challenges that can strengthen the AM in the manufacturing field is the elimination of post-processing, in particular, improving the dimensional accuracy, surface finishing and mechanical properties. Though, inaccuracy of dimensions cannot be neglected nor the mechanical strength in most engineering fields, contrarily, these two are most needed in biomedical, aerospace or any industry that requires specific fits and tolerances. Being able to print accurate 3D-geometries as demanded is one of the goals to be achieved in AM, particularly FDM. Finally, the optimization of FDM printed parts' dimensional quality, surface and mechanical strength will greatly contribute in supporting many fields like complicated surgeries for unique patient-customized products [2], [3], micro and nano-electronics, automotive industry [12], ...etc. There are many other researches that are conducted on the optimization of FDM process like building time and material behavior, however, dimensional accuracy, final surface quality and mechanical properties were found more critical to be optimized.

## 1.2. Problem Statement

The evolution of the FDM process amongst conventional manufacturing techniques is about to be achieved. Can the optimization of FDM final product quality and the other variable outputs place it as a competitive manufacturing technique? It is a wonder whether the FDM process

can reach an acceptable level of accuracy compared to the current state of manufacturing techniques accuracy. Meanwhile, the FDM process outputs are extremely unpredictable, though, if the involvement of a large number of parameters is achievable, can this adjust the uncertainty of the process?

### **1.3. Thesis Objectives**

The objective of this research is to develop an optimization model that relates the maximum possible number of printing parameters to the dimensional accuracy, surface and edge quality of the 3D printed parts and searches for the optimum parameters. This can be concluded in the following:

1. Gathering as much as possible parameters that are studied in the literature.
2. Developing a DOE model of these parameters in order to develop a reliable model that is derived by these parameters and relates them to the outputs.
3. Testing the model on experimental basis on a 3D printer using FDM approach.
4. Conducting analysis of variance ANOVA in order to check the fitness of the developed model to promote it as an optimization model.
5. Developing a multi-objective optimization model considering maximum number of parameters.
6. Validating the optimal parameters to the developed experiment-based model.

### **1.4. Thesis Layout**

The first chapter take a leap insight into the history of additive manufacturing AM since its birth. Also, a glance about the categories of AM techniques is presented, while the addressed technique FDM is one of the solid based AM techniques. In addition, a brief description of the FDM process is explained. Eventually, the objectives of this thesis are highlighted. In the

following chapter, the exploration of printing parameters and their influence on the FDM variable outputs is conducted. Mainly, the review of the literature focuses on the dimensional accuracy and appearance quality of the FDM 3D printed parts. Next, in chapter three, the experimental work of this thesis is presented. This chapter includes the experiment setup and used material, also, the design of experiment and running procedure are presented. At the end of this chapter, the measurements of the outputs are illustrated and explained carefully, in addition to the measuring tool used. Chapter four starts with the presentation the results of the conducted experiment tests. Then, ANOVA analysis is conducted on the effect of parameters on the outputs followed by the quadratic regression modeling of the mathematical experiment-based model on MATLAB 9.10 2021a [16]. The final part of the chapter includes the multi-objective optimization model of the extracted mathematical model from chapter 4, which is discussed and analysis in detail. The final chapter presents the outcomes and conclusions of the thesis, in addition to the require investigation and recommendations for future work.

## CHAPTER TWO: LITERATURE REVIEW

Fusion deposition modelling is a 3D printing method, while 3D printing is one of the AM techniques. The definition “fused deposition modelling (FDM)” comes from the process itself by depositing semi-molten, or fused, material in layers form in top of each other [5], [6], [17]. Thermoplastics like, acrylonitrile-butadiene-styrene (ABS) and polylactic acid (PLA), are considered to be the most commercial used materials in FDM because they result in good mechanical properties of the output, and they are considered safe to the environment [18]. Although, there are various remarkable investigations done on new materials to be added to the FDM materials paradigm [3], [19]. The printing parameters of FDM and their impact on the quality and strength of the output parts were discussed in depth in [2], [5], [6], [20]–[26]. For example, build orientation, nozzle diameter by which other parameters like layer thickness, contour width, number of contours and raster width are determined, raster angle, infill density, extruder and printing chamber temperature, toolpath and the distance between the nozzle tip and the in-process layer. Although, the literature shows that FDM is capable of fabricating complex 3D geometries in many industries with lower cost on reasonable time [12], Oropallo et al. [11] and Ngo et al. [3] listed in their studies the critical limitations that make FDM hinder behind. Unlike any other process of 3D printing, because FDM suffers from the absence of supporting medium for the in-process printed part, and it is considered a material extrusion process, therefore many considerations are to be taken before processing. According to [2], in order to achieve the desired quality of the output, complicated procedures to calculate the printing parameters and surrounding conditions are considered by engineers. Masood [27] proposed a framework called intelligent rapid prototyping (IRP) which helps in the determination of all the printing parameters starting from the design for 3D printing on CAD software until the selection of nozzle diameter and the optimization of the extruder road

parameters. This IRP framework showed improvement in the efficiency and productivity of FDM, not only that, but also the quality of the printed products. The most remarkable parameters found in the review which has been experimented and simulated in order to relate their influence on the final product dimensional accuracy and surface finish are build orientation, layer thickness (or height), forced cooling, printing speed, toolpath (or deposition pattern), temperature, and infill density.

An experimental study on a modified commercial 3D printer was presented by Lee and Liu [14]. The modification they have added was an extra cooling system attached to the extruder of the 3D printer. Though, the parameters that were tested are air cooling speed and building orientation of the part on the printer platform. This study demonstrated that building direction has a good influence on dimensional accuracy, also mechanical properties when the layers are built in the transverse direction. For the cooling speed, it showed that zero and very high cooling speed result in high dimensional accuracy errors, and it is optimum to keep the cooling rate moderate, while Costa et al. [28] showed lower cooling rates lead to good surface finish but inferior dimensional quality. In addition, another optimization model was developed by Pandey et al. [29] using non-dominated sorting genetic algorithm II (NSGA II). The model highlighted that orientation of the part is the most important factor to obtain good surface finish. Moreover, the building orientation showed significant influence on dimensional quality and repeatability in [30]. Furthermore, in a computational simulation performed by Armillotta [15] to study the effect of three different angles on the platform of the 3D printers considering radius of sharp edges and staircase effect in addition to the layer thickness on final part quality. This simulation concluded that proper positioning of the part will help in the avoidance of edge errors and swelling of layers. The influence of building orientation on dimensional accuracy and surface roughness has not appeared to be low in the literature even in the most recent

review in [2]. Contrarily, it is one of the most influential parameters on final part geometrical accuracy.

The second noticeable influencing parameter is the layer thickness (LT). In 2001, a Taguchi model optimization was developed by Anitha et al. [25] on LT, printing speed and road width. After obtaining the optimum parameters, statistical analysis was performed using Analysis of Variables (ANOVA) and Signal to Noise (S/N) ratio to verify the results from the model. The analysis showed that LT has a high significant effect on surface finish and dimensional accuracy whether there is a pooling with other parameters or not. Moreover, Taguchi's approach research was proposed by Moza et al. [31]. LT was experimented by FFF Duplicator 4X 3D printer to have a good influence on dimension quality in z-direction rather than x-y plane. Furthermore, combining Taguchi's method with fuzzy logic technique showed that part orientation and LT are the most affecting parameters in the FDM printing process [32]. Recently, another experimental optimization model was presented by Alafaghani et al. [8] in 2017. Also, the model proposed a new design for manufacturing or FDM approach by using finite element analysis FEA. The parameters involved in this research are layer thickness LT, building pattern, extrusion temperature, printing speed and infill density. The results of this study showed that good final part dimensions are greatly influenced by LT, temperature and building pattern. In addition, they suggested that the critical dimension in the printed part should be parallel to the layer orientation using low extrusion temperature and higher LT. In [5], LT and staircase effect were related in an intuitive concept. That is the more sliced layers (lower LT) the best dimension quality can be obtained. More parameters beside the LT were examined in Pérez et al. [33], printing speed, temperature, wall thickness (WT) and toolpath (concentric, zig-zag, grid). This examination was carried out through an experiment on FDM printed samples. Thus, ANOVA revealed that LT and WT are combined factors that enhance surface quality. If one of the latter two increases while the other is fixed, or both increase

greatly, that results in low surface quality. More revelation, the toolpath or printing path had a low impact on the quality of the surface. Remarkable recent research is conducted to investigate the effect of layer thickness, filament color, raster angle and build orientation on the accuracy of dimensions in the FDM process. The experimental tests are performed on cylinders and dog bone shapes, as shown in Figure 3, on a commercial 3D printer. The results are unexpected that the filament color shows high impact on the dimensional accuracy of both samples geometry. Also, the layer thickness LT and build orientation dominated other parameters to affect the quality of the final output. However, the raster angle is found to have no impact on dimensional accuracy [34].

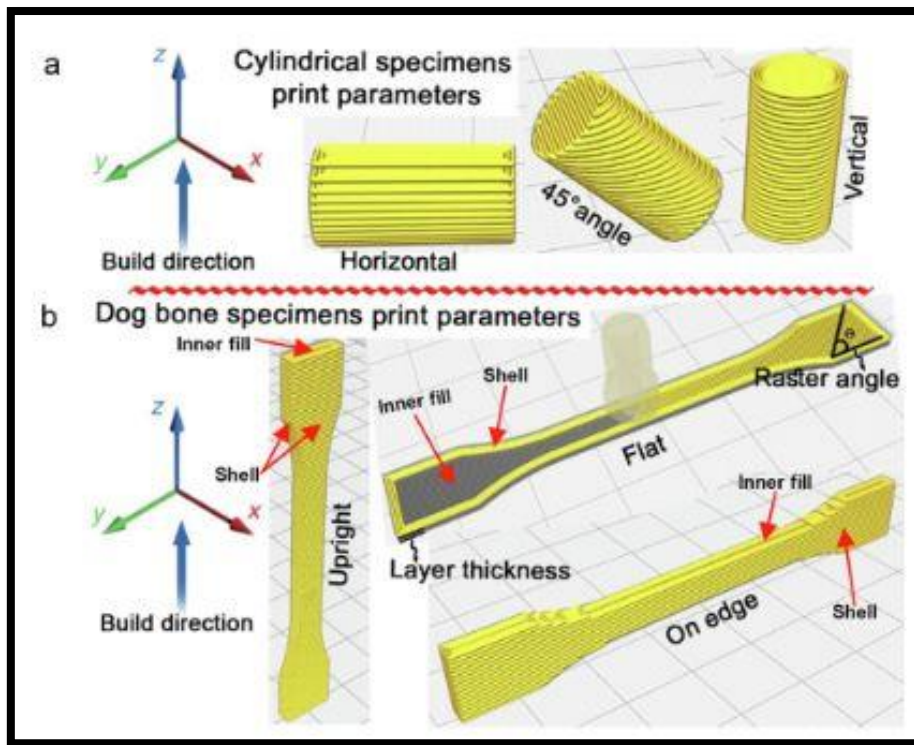


Figure 3: (a) Print orientation of cylinder parts, and (b) parameters used to print dog bone samples [34].

Another impressive experimental-based study on the effect of five printing parameters on the dimensional accuracy and surface quality of the FDM printed parts is carried out using Taguchi array (L50) DOE [35]. The PLA test samples included various geometries in order to

investigate the dimensional accuracy as illustrated in Figure 4. Surprisingly, the most influential parameters on dimensional accuracy and surface quality are the layer thickness (LT) and printing speed. To conclude, LT has always been an obvious parameter that affects the quality of surface or dimension accuracy, particularly on edges or curved surfaces [1].

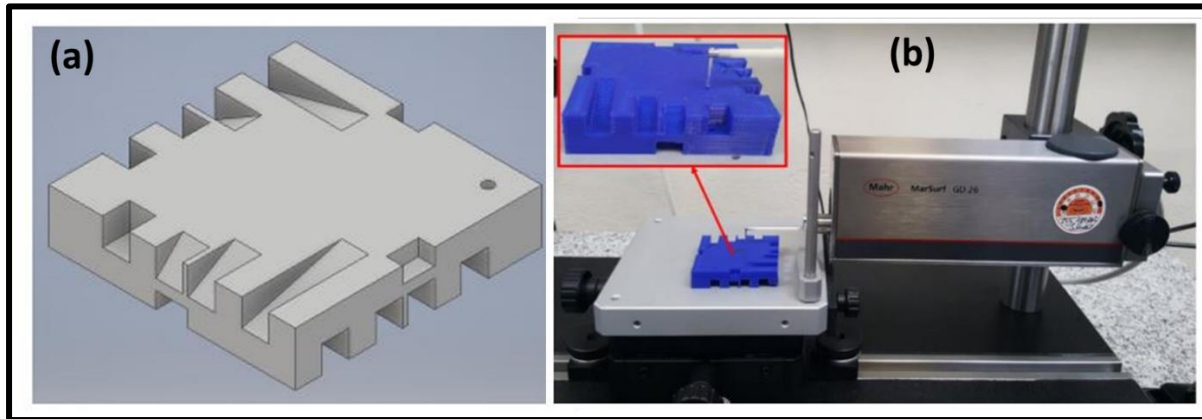


Figure 4: (a) CAD model of test sample including various geometries, and (b) final printed samples [35].

As for the other printing conditions, temperature investigations have contradictory opinions. In [28], it was concluded that envelope temperature is a critical parameter as it has some beneficial characterization which is the lasting effect. Moreover, as mentioned previously in [8], proper selection of temperature produces fine dimensional accuracy. On the other hand, temperature compared to LT and build orientation has a lower influence on geometry quality [33]. Also, there have been many corrections operated on the slicing software output parameter, which is the .STL file. Roschli et al. [1] showed the limitations facing the slicing process, especially for curved 3D models. Meanwhile, a compensation method on STL files is applied on two different machines, FDM 3000 and SLA 50. The correction of the STL file showed 30% reduction in the volumetric error due to shrinkage in FDM 3000 rather than the SLA 50 with smaller error reduction [36]. Other parameters like infill density have lower influential sense on dimensional accuracy and surface quality, however it records higher expectations on mechanical properties [8], [22].



## Research Aims

Most studies reported in the literature were carried out through optimizing from three up to six printing parameters and analyzing the influence of these parameters on the objective, which is usually a single or double objective. Meanwhile, the other printing parameters and conditions were set as fixed values. Unluckily, the results often showed that often two parameters, which are building orientation and layer thickness, are the most influential to the output. In this thesis as an initial step, most of the effort will be exerted on investigating and maximizing the usage of other parameters. The literature offers various parameters that affects the dimensional accuracy and surface quality of the FDM prints, hence, in this research, the selected printing parameters as follow; layer height, wall thickness, bottom/top thickness, infill density, temperature and printing speed. Following, experimental work will be operated upon those parameters. Finally, a multi-objective optimization model will be developed considering the maximization of printing parameters, or decision variables in order to enhance the dimensional accuracy, edge quality and surface quality of the 3D printed parts by FDM.

# CHAPTER THREE: EXPERIMENTAL WORK

## 3.1. Equipment Setup and Material

The material used in this research is polylactic acid plus (PLA+) filament of 1.75 mm diameter. The filament is purchased from SHENZHEN eSUN industrial CO., LTD with a manufacturer recommendations of best practice printing parameters as printing temperature of 205-220 °C and the heated bed temperature of 25-70 °C. The physical and mechanical material properties are presented in Table 1. The selected filament colour is brown as shown in Figure 5.

Table 1: Physical and mechanical properties of (PLA+).

Density (g/cm <sup>3</sup> )	Heat Distortion Temp (°C, 0.45MPa)	Tensile Strength (MPa)	Elongation at Break (%)	Flexural Strength (MPa)	Flexural Modulus (MPa)	IZOD Impact Strength (kJ/m <sup>2</sup> )
1.24	56	65	8	97	3600	4



Figure 5: Brown color PLA+ filament of 1.75mm diameter.

In this research, a custom-made commercial 3D printer MakerX Pro 200mm x 200mm is used in the experimental operation. The machine chassis and structure are produced from aluminium sheet metals of 1.25 mm thickness and aluminium V-shaped cross-section. A 24V heated bed is installed on the printer machine that can reach 110 °C. The installed stepper motors are Nema 17 high torque. For the controller unit, it is combined of ramps 1.4+ Arduino Mega 2560 + a4988 drivers. The hot end type is E3DV6, while the extruder type is MK8. Overall, the machine can reach 50 µm resolution. Regarding the movement of the axes of the machine, the build bed is mounted on Y-axis, and moves forward and backward while remaining at  $Z = 0$ . The X-axis is assembled on a V-shape cross-section member that is moving left and right starting from  $x=0$ , meanwhile, the X-axis subassembly is coupled with the Z-axis movement through a power screw of 5 mm diameter, hence, the Z-axis movement carries the X-axis subassembly along. Though, the printed part is built from zero layer to the final layer without moving the build bed up. The details of the machine components and movements are presented in Figure 6.

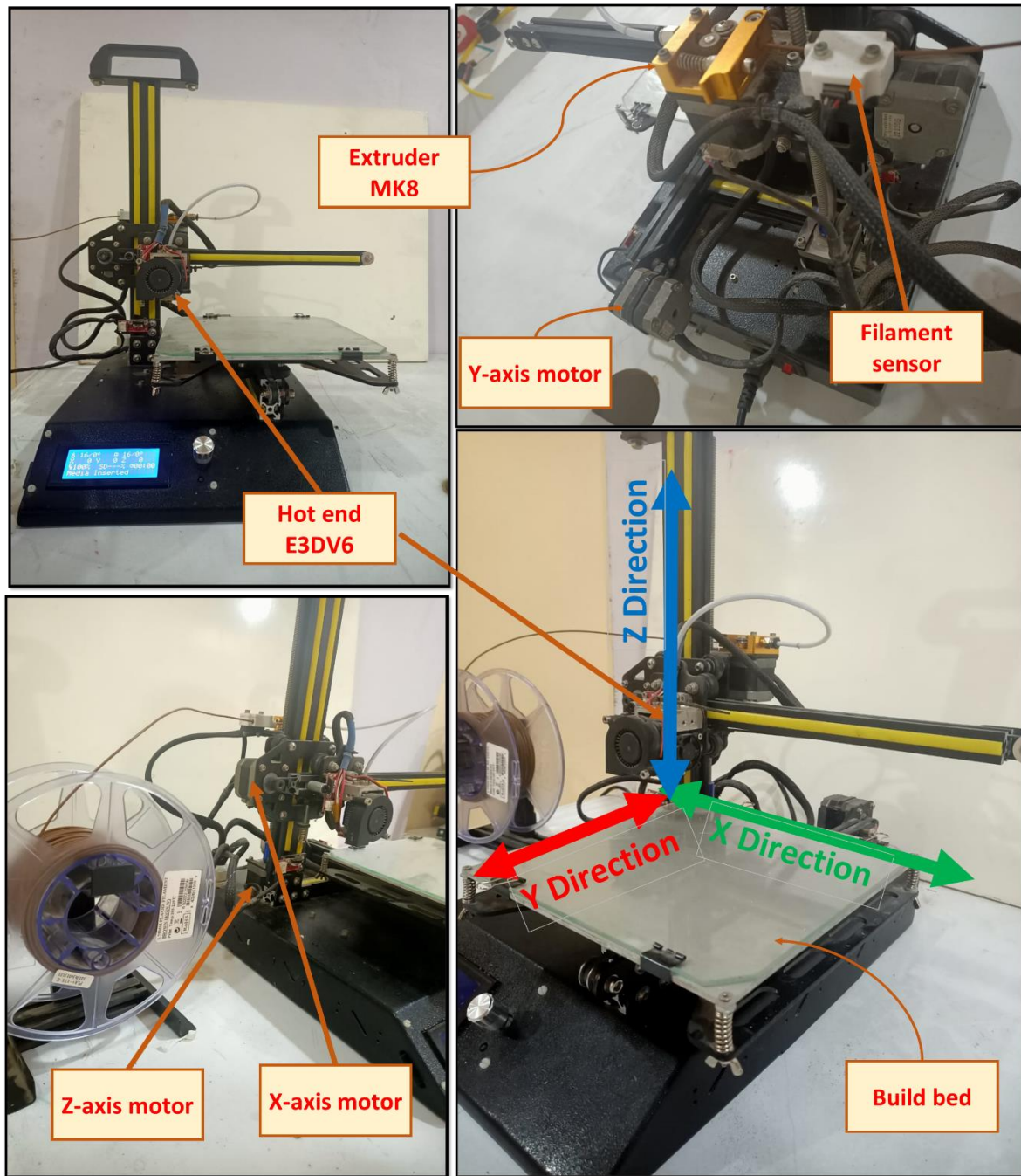


Figure 6: MakerX Pro 3D printer details.

### 3.2. Design of Experiment (DOE)

In this study, involving a larger number of printing parameters in one experimental-based mathematical model is of interest. The effect of each parameter individually on variable outputs of the FDM process is minimal. Though, the effect of the interaction between printing parameters is addressed. The selected printing running conditions are layer height  $LH$  (mm),

wall thickness  $Wt$  (mm), bottom/top thickness  $BTt$  (mm), infill density  $InD$  (%), temperature  $T$  ( $^{\circ}C$ ) and printing speed  $V$  (mm/s). The selection is based on the outcome of the review of the literature as these parameters are the most highlighted influential conditions on the FDM process. Meanwhile, the DOE is selected to be a 2-level full-factorial design. The parameters levels are presented in Table 2. Consequently, the experimental tests that are conducted in this research are  $2^6$  tests for each case of different geometry; cube and cylinder, which means 128 test samples. The cube is 20x20x20 mm, and the cylinder is 20 mm diameter and 20 mm height. However, the single test included a cube and a cylinder in order to assure that the parameters set and conditions are fixed for both geometries as shown in Figure 7, hence, the uniaxial and biaxial movement of the printing hot end are tested simultaneously.

Table 2: Table of parameters and levels.

Parameters	Levels	Unit
Layer height ( $LH$ )	[0.1 0.2]	mm
Wall thickness ( $Wt$ )	[0.4 1.2]	mm
Bottom/top thickness ( $BTt$ )	[0.8 1.6]	mm
Infill density ( $InD$ )	[25 50]	%
Temperature ( $T$ )	[190 210]	$^{\circ}C$
Printing speed ( $V$ )	[30 60]	mm/s

The selection of the levels of temperature and printing speed parameters considers one level inside the manufacturer recommendation, and the other level is below the lower bounds. For the layer height levels, the used nozzle diameter is 0.4 mm, hence the layer height is preferred not to exceed 0.2 mm. Meanwhile, the infill density of greater than 50% has no further effect on dimensional accuracy and final part appearance quality, unless the mechanical properties are addressed to be enhanced. The last two parameters' levels; wall thickness and bottom/top thickness, are selected based on experimental trials on previously printed samples.

### 3.3. Parameters and Slicing

Although the selected number of parameters are quite large, however, some primary parameters are assumed constant. For example, the nozzle diameter, the heated bed temperature, the type and geometry of used filament, cooling rates, initial layer height, infill pattern and wall speed are fixed parameters through all the experimental tests, except wall speed is set to be equal to the printing speed. The fixed parameters are presented in Table 3.

Table 3: Fixed running conditions.

Fixed Conditions	Value	Unit
Nozzle diameter	0.4	mm
Bed temperature	65	°C
Filament	PLA+	mm
Filament diameter	1.75	mm
Cooling rates	No cooling	-
Initial layer height	0.2	mm
Infill pattern	Grid	-
Wall printing speed	Equal printing speed ( $V$ )	mm/s
Brim width	4 (10-line count)	mm

In order to construct a 3D model in the format of .STL file, SolidWorks 2020 [37] is used. While, the used slicer software is Ultimaker Cura 4.12.1 [38]. In Figure 7, a preview shot of the Cura software slicing process is illustrated. The preview mode shows the building progress of the printed samples before starting the process. Mainly, the 3D model is exported to the .STL file extension that is the input file for the slicer software. Then, Cura generates a .gcode file in order to operate the 3D printer similar to any other CNC machine.



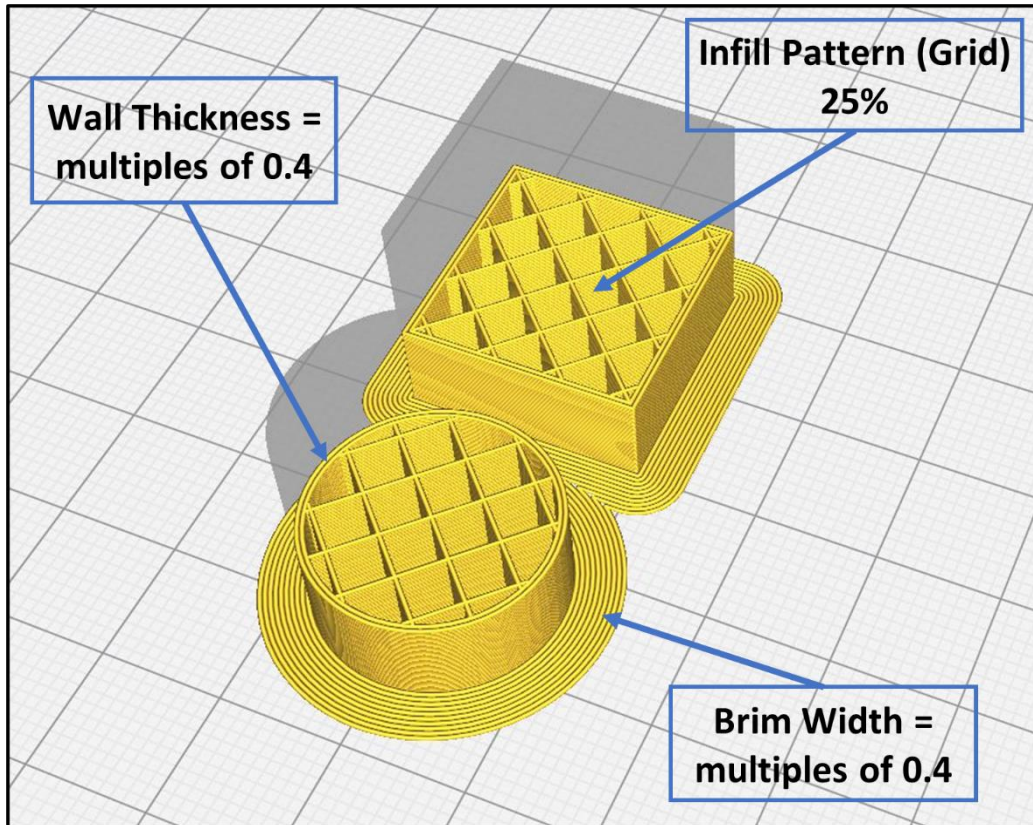


Figure 7: Ultimaker Cura slicing preview mode (Copyrights reserved to Ultimaker company).

### 3.4. Measurements and Measurement Tool

At this stage, the final parts are measured on the basis of main axial dimensions  $[x\ y\ z]$  and planer dimensions  $[xy\ zx\ zy]$ . In case of cube samples, 16 measurements are collected out of each cube. The considered dimensions of the cube are shown in Figure 8. Three dimensions for  $x$  and  $y$ , three dimensions for  $zx$  and  $zy$  planes, and four dimensions for the  $z$  direction are measured as shown in Figure 8. The center of the cube is determined by the intersection of the  $x$  and  $y$  faces diagonals.

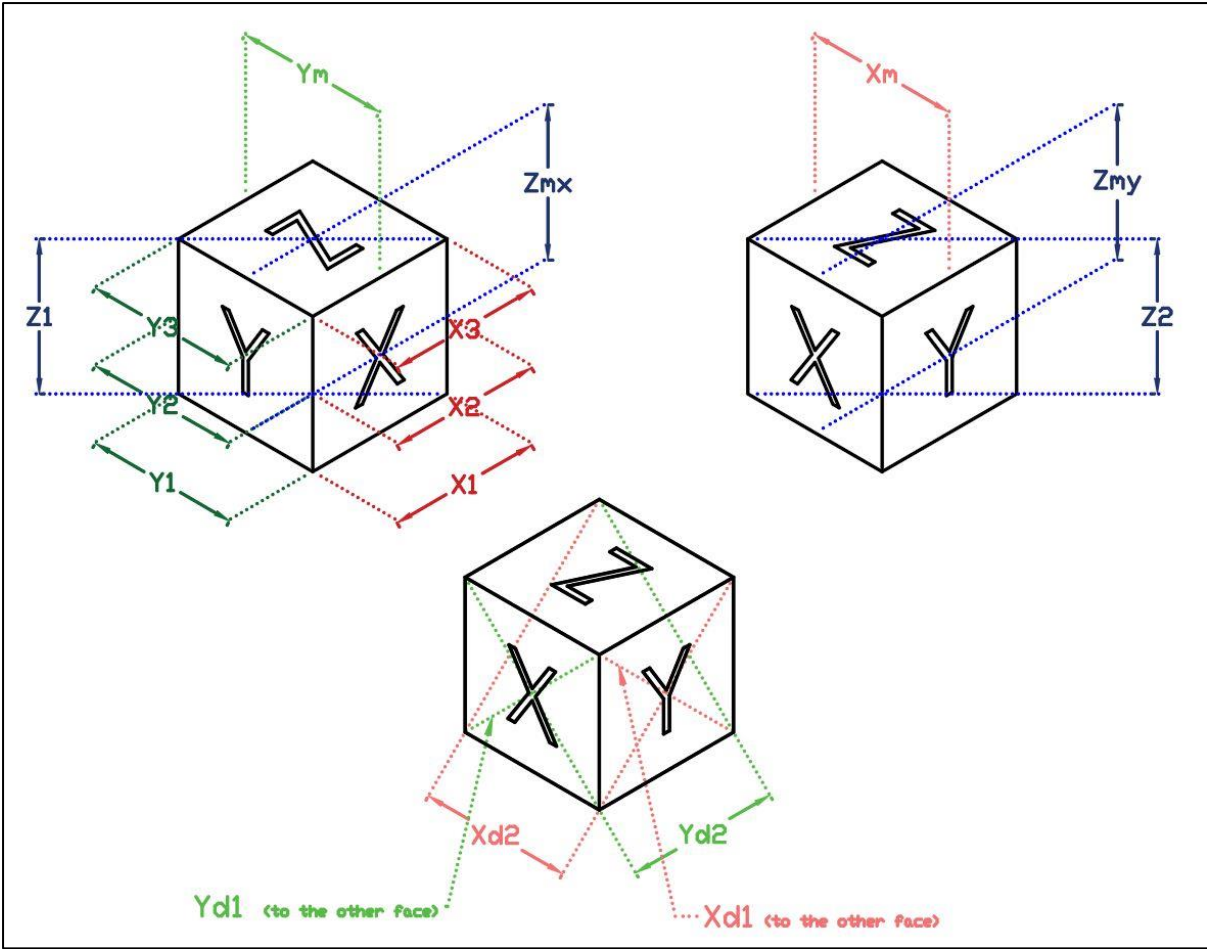


Figure 8: Measured cube dimensions.

The other case of cylinders, the measurement of 9 dimensions, three for each axis  $x$ ,  $y$  and  $z$  is performed. These dimensions are illustrated in Figure 9. Overall, the measurement of these dimensions is input independent for the dimensional variation output. The measurement tool is INSIZE digital caliper “Code 1108-150” that can measure up to 150 mm with a resolution of 0.01 mm, see Figure 10.



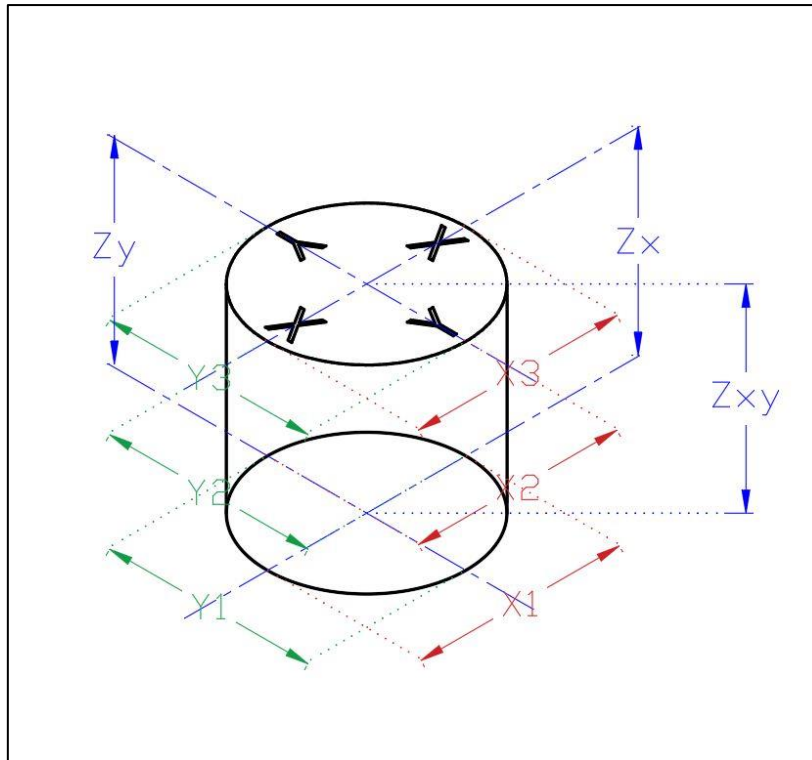


Figure 9: Measured cylinder dimensions.



Figure 10: INSIZE digital caliper "Code 1108-150".

For the other two output variables; edge quality and surface quality, a level of scores is considered. The edge quality score levels are the interval [0 3], while the surface quality interval is [0 5]. Before mentioning how these levels are calculated, the edge and surface defects are discussed. The objective of edge and surface quality outputs is to enhance the defects that occur during the printing process. In this study, 3 edge defects and 5 surface defects are addressed. The edge defects are the appearance of elephant foot “so called blistering”, curling or rough edges and warping edges. The elephant foot occurs when the recent printed

layers solidifies faster than the base layers. Also, the curling or rough edges is the appearance of wavy edges or saw tooth shaped edges. Whenever the bed temperature is not sufficient to adhere the initial layer to the build plate, the warping of edges takes place. In addition, the surface defects are top surface finish “appearance of gaps or incomplete surface”, staircase phenomena, surface waviness “ghosting”, under/over extrusion and layer cracking. The edge and surface defects are categorized in Figure 11 and Figure 12. Hence, each defect is given an equal score of 1.

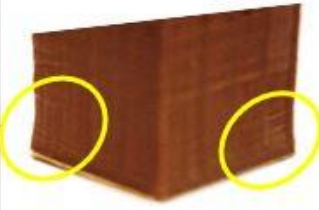





Objective	Defect	Cube	Cylinder
<b>Edge Defects</b>	<b>Elephant foot (blistering)</b>		
	<b>Curling (Rough corner)</b>		
	<b>Warping</b>		

Figure 11: Printing parts edge defects.

The edge quality is determined by (1).

$$Edge\ Quality = 3 - \sum edge\ defects \quad (1)$$

While the surface quality is determined by (2).

$$\text{Surface Quality} = 5 - \sum \text{surface defects} \quad (2)$$



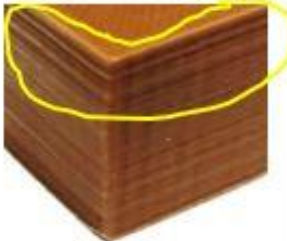







Objective	Defect	Cube	Cylinder
<b>Surface Defects</b>	<b>Top surface finish</b>		
	<b>Stair case</b>		
	<b>Surface waviness</b>		
	<b>Under/over extrusion</b>		
	<b>Cracking</b>		

Figure 12: Printing parts surface defects.

# CHAPTER FOUR: RESULTS AND DISCUSSIONS

## 4.1. Results of Cube Samples

As mentioned before, a number of 16 dimensions is measured for each cube. Then, the obtained dimensions are reshaped in the matrix form as follow:

$$Dimensions_{cube} = \begin{bmatrix} x_1 & y_1 & z_1 & x_{d1} & y_{d1} \\ x_2 & y_2 & z_2 & x_{d2} & y_{d2} \\ x_3 & y_3 & z_3 & x_m & y_m \end{bmatrix}$$

Where  $z_3$  term in the previous matrix is the average of  $z_{mx}$  and  $z_{my}$ .

After that, the standard deviation for each column is calculated in a vector form as follow:

$$S_{cube} = [S_x \quad S_y \quad S_z \quad S_{xd} \quad S_{yd}]$$

In order to reach an indicator of the dimensional variation, the Euclidean norm [39] of the standard deviation column is calculated. Let  $DV_{cube}$  be the dimensional variation of the cube:

$$DV_{cube} = norm(S_{cube}) = \sqrt{S_x^2 + S_y^2 + S_z^2 + S_{xd}^2 + S_{yd}^2}$$

The results of the edge quality and surface quality are obtained from the score matrices mentioned in the previous chapter. The final results of cube samples are shown in appendix (A).

## 4.2. Results of Cylinder Samples

Similarly, the obtained dimensions from each cylinder are reshaped in a matrix form. Unlike the cube samples, the faces diagonal  $x_{di}$  and  $y_{di}$  dimensions are neglected; hence, the matrix size is 3x3 accommodating for the three dimensions only as follow:

$$Dimensions_{cylinder} = \begin{bmatrix} x_1 & y_1 & z_1 \\ x_2 & y_2 & z_2 \\ x_3 & y_3 & z_3 \end{bmatrix}$$

Where  $z_3$  is the average of  $z_x$  and  $z_y$ .

Again, the standard deviation of each column is calculated in a vector form, also, the Euclidean norm of the standard deviation vector is calculated to obtain the dimensional variation of each cylinder as follow:

$$S_{cylinder} = [S_x \quad S_y \quad S_z]$$

$$DV_{cylinder} = norm(S_{cylinder}) = \sqrt{S_x^2 + S_y^2 + S_z^2}$$

The other required results are obtained from the score matrices. The complete results of the cylinder samples are presented in appendix (B).

### **4.3. Analysis of Variance (ANOVA)**

In this section, the analysis of the relationship between the results and the parameters is illustrated in detail. This analysis is carried out by using MATLAB 2021a and Minitab 19.1 software [40]. The analysis of the cube and cylinder model is performed separately. First, the main effects of parameters on the desired results are plotted on Minitab in order to visualize the influence of the parameters on each result. Then, a quadratic regression method on MATLAB is used to obtain the regression fit of the parameters and results. Finally, the normal probability of residuals, the histogram of residuals and the parameters interactions are plotted for each regression model.

#### **4.3.1. CUBE MODEL ANALYSIS**

The main effects of parameters on dimensional variation, edge quality and surface quality are plotted in Figure 13, Figure 14 and Figure 15, respectively.

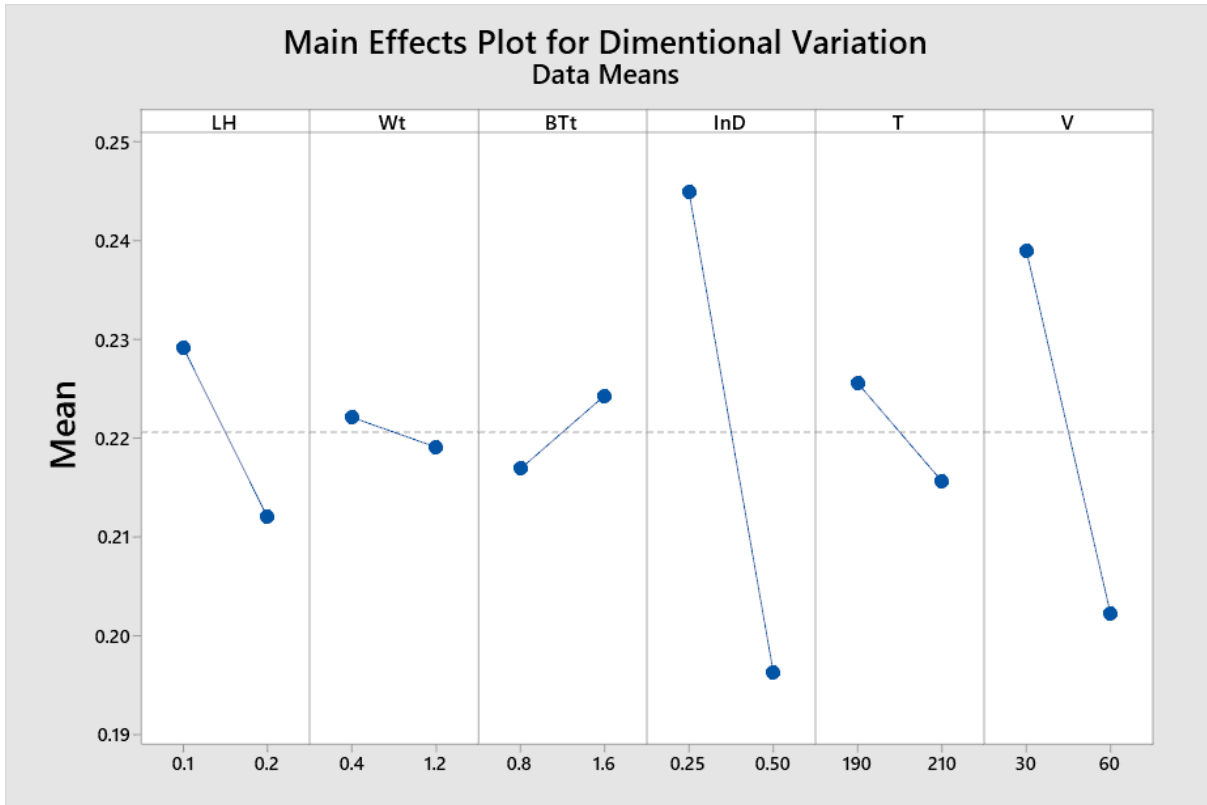


Figure 13: Main effects plot for dimensional variation of cube samples.

The main effects plot shows that the most effective parameters on the dimensional variation of cube samples are infill density  $InD$ , speed  $V$  and layer height  $LH$  in order. Surprisingly, the three parameters attain the same disproportional behavior to the  $DV_{cube}$ , as it decreases with the increase of each parameter. Meanwhile, the edge quality is affected greatly by layer height  $LH$  followed by infill density  $InD$  and temperature  $T$ . Unlike the  $DV_{cube}$ , the parameters are proportional to the output. Last, the surface quality of cube samples is influenced by wall thickness  $Wt$  remarkably, in addition to the speed  $V$  and layer height  $LH$ .

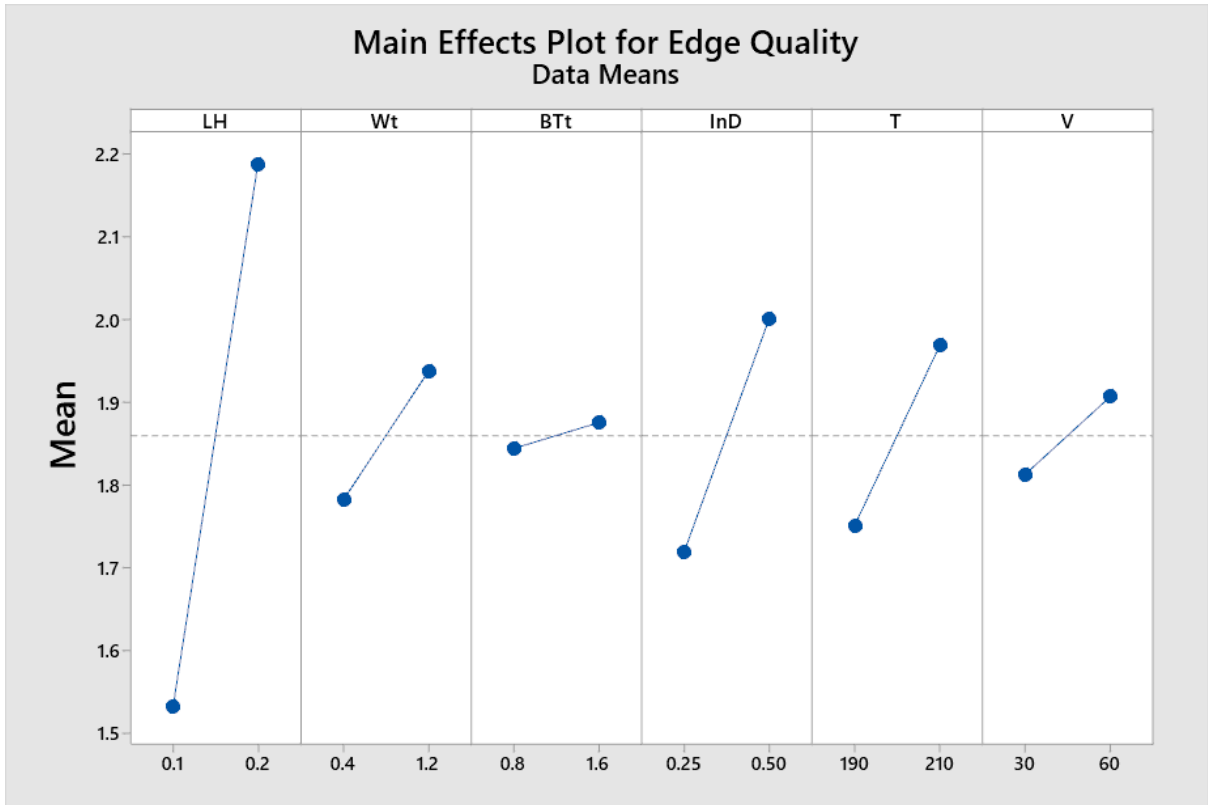


Figure 14: Main effects plot for edge quality for cube samples.

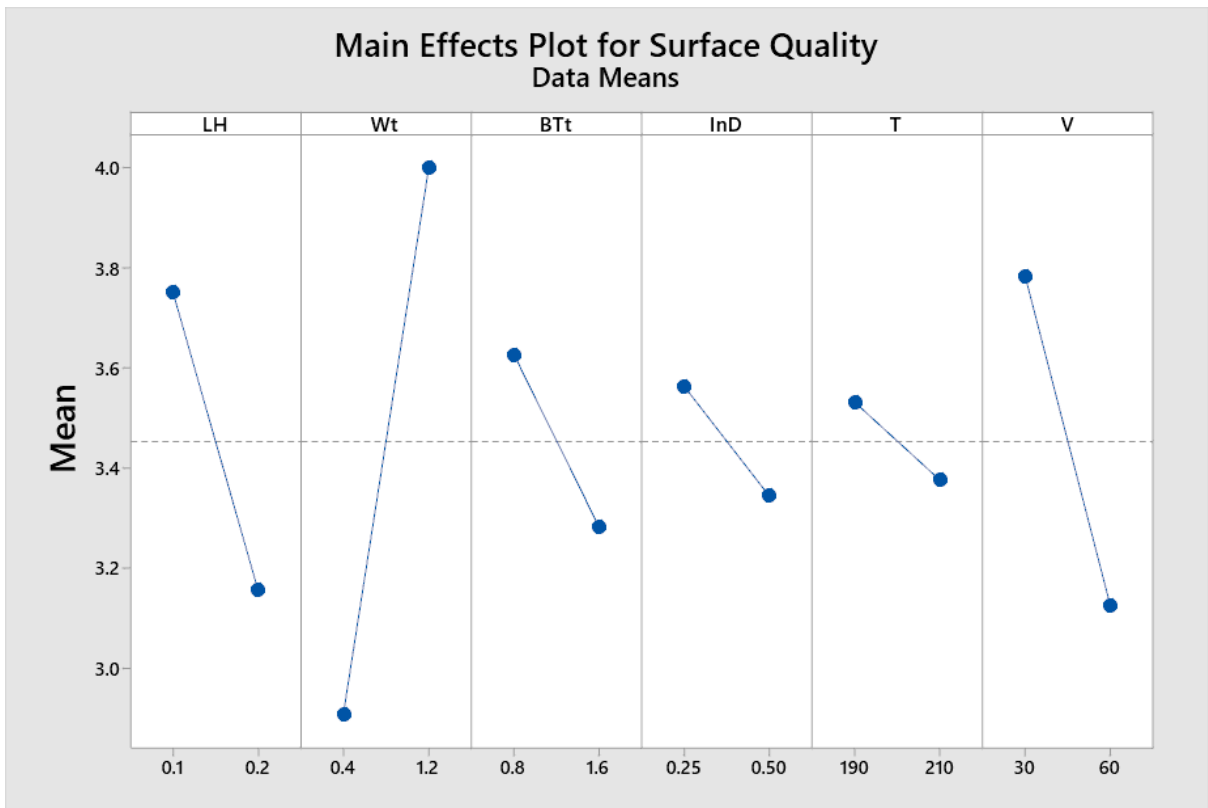


Figure 15: Main effects plot for surface quality for cube samples.

Next, the quadratic regression model is developed by MATLAB for each output. In order to enhance the model behavior, the parameters are normalized to an interval value of [-1,1] as shown in (3). Hence, all parameters are given the subscript  $n$  for normalization.

$$\hat{x} = 2 \frac{x - \min x}{\max x - \min x} - 1 \quad (3)$$

The first output ( $DV_{cube}$ ) is shown in (4). The regression R-Square is 70.5% with a  $p$ -value of 0.026. The ANOVA table of the first output is presented in Table 4. The table shows that the most significant terms in the model are  $InD_n$ , the interaction between  $Wt_n V_n$  and  $V_n$  with  $p$ -values of 0.003414, 0.009752 and 0.02317, respectively.

$$\begin{aligned} DV_{cube} = & 0.2206 - 0.0243InD_n - 0.0212Wt_nV_n - 0.0184V_n \\ & - 0.0156Wt_nT_n + 0.01383Wt_nBTt_n + 0.01316InD_nV_n \\ & + 0.01012LH_nInD_n - 0.01004Wt_nInD_n \\ & + 0.00952LH_nBTt_n - 0.0086LH_n - 0.007BTt_nV_n \\ & + 0.00678InD_nT_n + 0.00573LH_nV_n - 0.005T_n \\ & + 0.00421LH_nWt_n + 0.00372BTt_n \end{aligned} \quad (4)$$

Table 4: ANOVA table of dimensional variation of cube samples.

	Estimates	SE	t-stat	p-value
Intercept	0.220602	0.007765	28.41061	3.00E-26
$InD_n$	-0.02434	0.007765	-3.13492	0.003414
$Wt_n: V_n$	-0.02119	0.007765	-2.72954	0.009752
$V_n$	-0.01842	0.007765	-2.37181	0.02317
$Wt_n: T_n$	-0.01563	0.007765	-2.0124	0.051705
$Wt_n: BTt_n$	0.013834	0.007765	1.781619	0.083249
$InD_n: V_n$	0.013165	0.007765	1.695432	0.098627
$LH_n: InD_n$	0.010125	0.007765	1.30391	0.200541
$Wt_n: InD_n$	-0.01004	0.007765	-1.2935	0.204078
$LH_n: BTt_n$	0.009525	0.007765	1.226658	0.227914
$LH_n$	-0.00861	0.007765	-1.10897	2.75E-01



$BTt_n: V_n$	-0.00704	0.007765	-0.90674	0.370576
$InD_n: T_n$	0.006784	0.007765	0.873738	0.388052
$LH_n: V_n$	0.005727	0.007765	0.737604	0.465536
$T_n$	-0.00498	0.007765	-0.6415	0.525263
$LH_n: Wt_n$	0.004212	0.007765	0.542468	0.590839
$BTt_n$	0.003716	0.007765	0.478557	0.635148

The normal probability of residuals plot is shown in Figure 16. Fortunately, the plotted residuals are close to the 45-degree line, which means the data have appropriate fit.

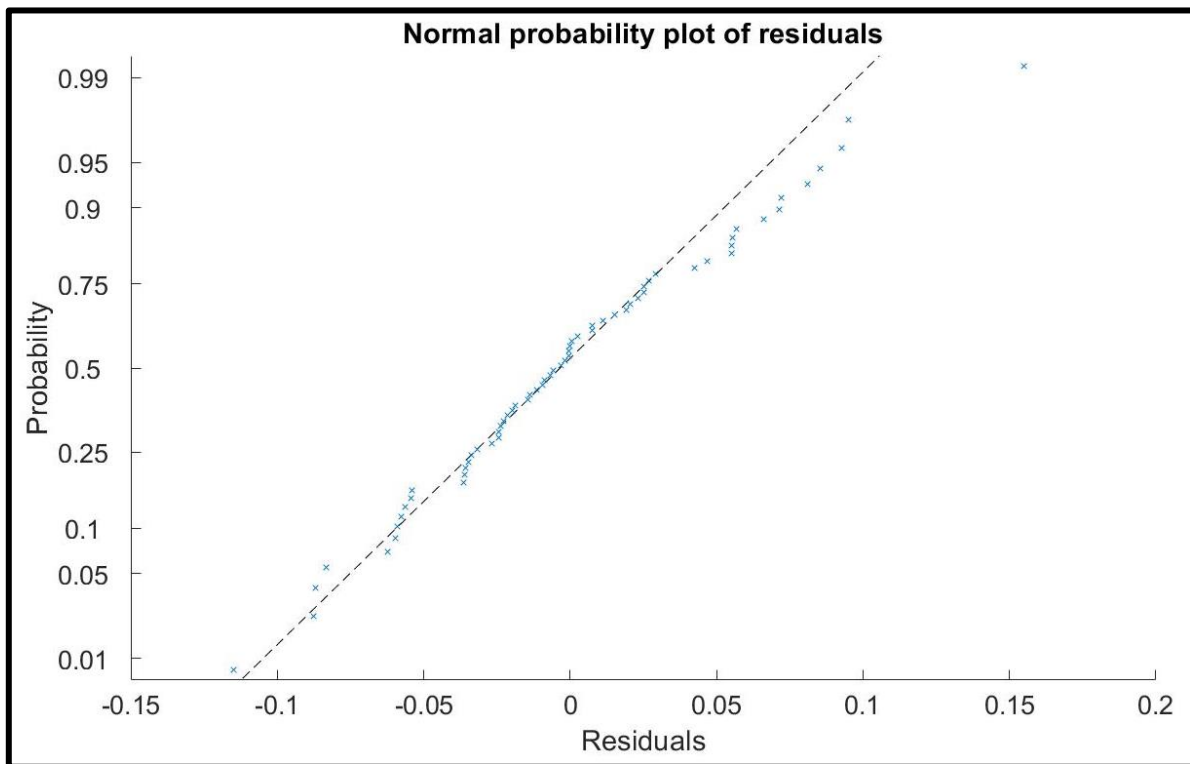


Figure 16: Normal probability plot of residuals for the dimensional variation regression of cube samples.

In order to check the fitness of the model, the histogram of residuals shows that the residuals are normally distributed as shown in Figure 17. Also, the interaction between all model parameters is plotted in Figure 18.

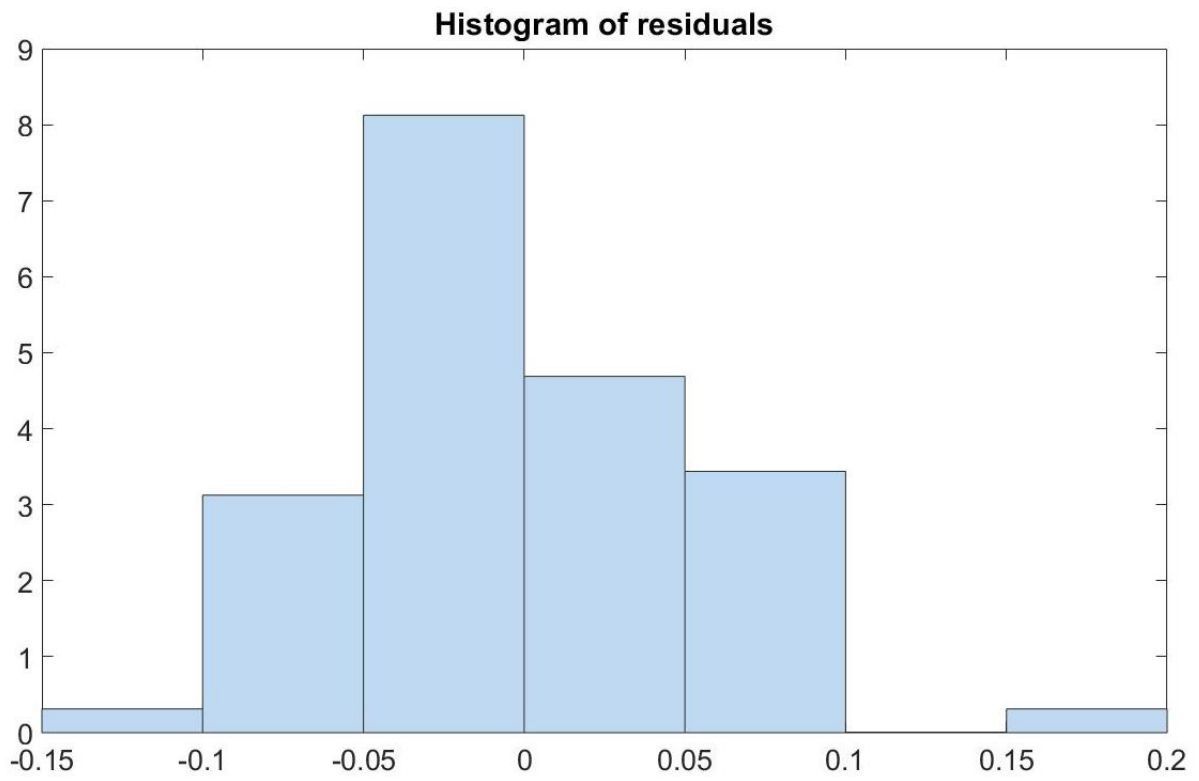


Figure 17: Histogram of residuals for the dimensional variation regression of cube samples.

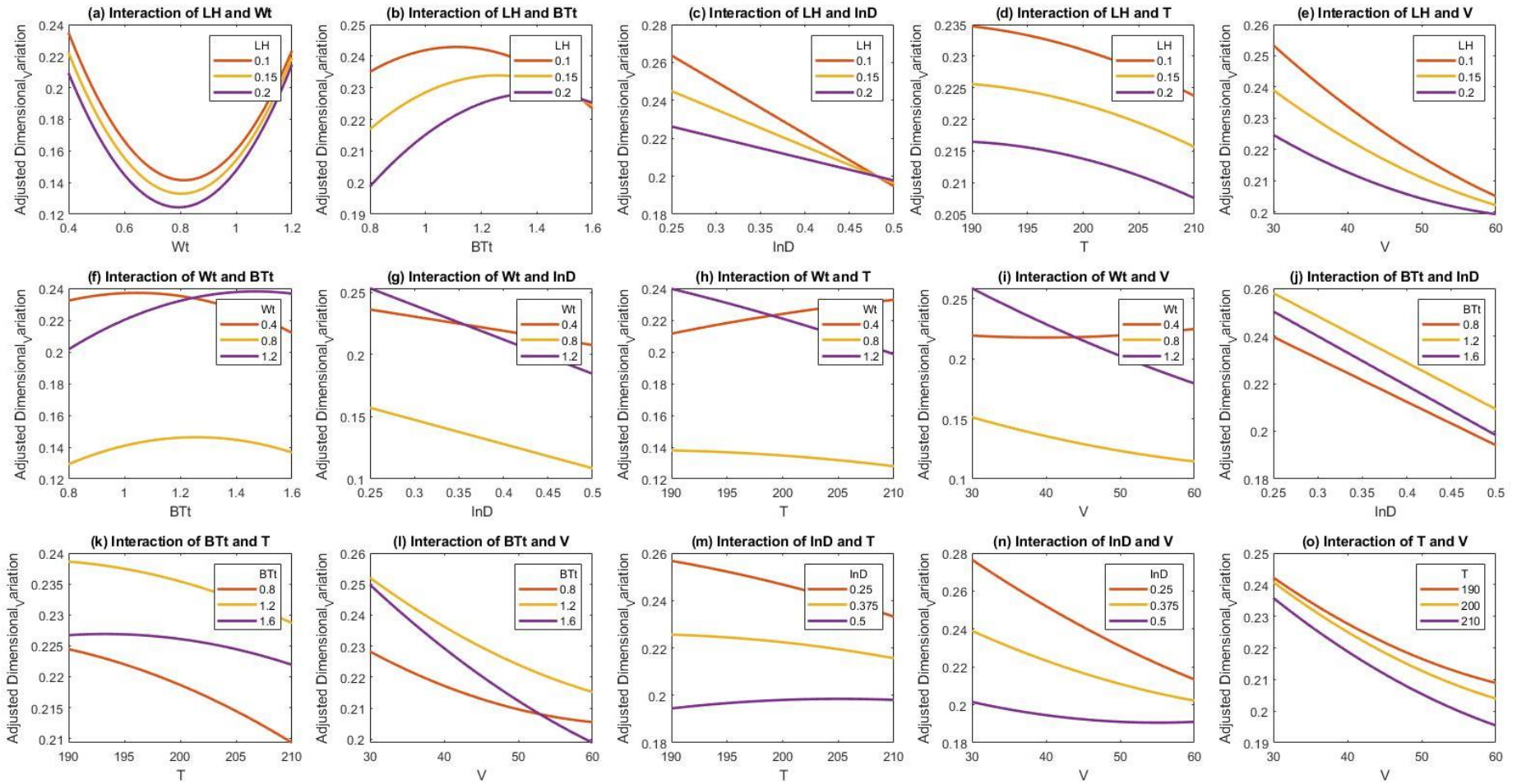


Figure 18: Parameters' interactions of the dimensional variation regression of cube samples: (a)  $LH$  and  $Wt$ , (b)  $LH$  and  $BTt$ , (c)  $LH$  and  $InD$ , (d)  $LH$  and  $T$ , (e)  $LH$  and  $V$ , (f)  $Wt$  and  $BTt$ , (g)  $Wt$  and  $InD$ , (h)  $Wt$  and  $T$ , (i)  $Wt$  and  $V$ , (j)  $BTt$  and  $InD$ , (k)  $BTt$  and  $T$ , (l)  $BTt$  and  $V$ , (m)  $InD$  and  $T$ , (n)  $InD$  and  $V$  and (o)  $T$  and  $V$ .

The next model regression of cube samples is the edge quality. The obtained quadratic regression model from MATLAB in (5) has R-Square of 69.6% and a  $p$ -value of  $4.13 \times 10^{-5}$ .

$$\begin{aligned}
 \text{Edge Quality}_{cube} &= 1.8593 + 0.3281LH_n + 0.3281InD_nV_n - 0.2968LH_nV_n \\
 &- 0.2968LH_nT_n + 0.2031Wt_nV_n - 0.1718InD_nT_n \\
 &+ 0.1406InD_n - 0.1406LH_nInD_n + 0.1093T_n \\
 &+ 0.0781Wt_n - 0.0781Wt_nBTt_n - 0.0781Wt_nInD_n \\
 &+ 0.0781Wt_nT_n
 \end{aligned} \tag{5}$$

Moreover, the ANOVA analysis of edge quality regression is shown in Table 5. Remarkably, the parameters  $LH_n$ , interaction between  $InD_nV_n$  and interaction between  $LH_nV_n$  has the first three place order in significance on the edge quality regression model of cube samples.

Table 5: ANOVA table of edge quality of cube samples.

	Estimates	SE	t-stat	p-value
Intercept	1.859375	0.079013	23.53258	1.88E-23
$LH_n$	0.328125	0.079013	4.152807	0.000193
$InD_n: V_n$	0.328125	0.079013	4.152807	0.000193
$LH_n: V_n$	-0.296875	0.079013	-3.7573	0.000608
$LH_n: T_n$	-0.296875	0.079013	-3.7573	0.000608
$Wt_n: V_n$	0.203125	0.079013	2.570786	0.014427
$InD_n: T_n$	-0.171875	0.079013	-2.17528	0.036256
$InD_n$	0.140625	0.079013	1.779775	0.083556
$LH_n: InD_n$	-0.140625	0.079013	-1.77977	0.083556
$T_n$	0.109375	0.079013	1.384269	0.174798
$Wt_n$	0.078125	0.079013	0.988764	0.329378
$Wt_n: BTt_n$	-0.078125	0.079013	-0.98876	0.329378
$Wt_n: InD_n$	-0.078125	0.079013	-0.98876	0.329378
$Wt_n: T_n$	0.078125	0.079013	0.988764	0.329378

The normal probability plot and histogram of residuals are plotted in order to confirm the fitness of the model as shown in Figure 19 and Figure 20, respectively. The normal probability plot shows that the data is scattered and close to the 45-degree line, in addition, the histogram

of residuals follows a normal distribution. Hence, the fitness of the available experimental data can be reliable.

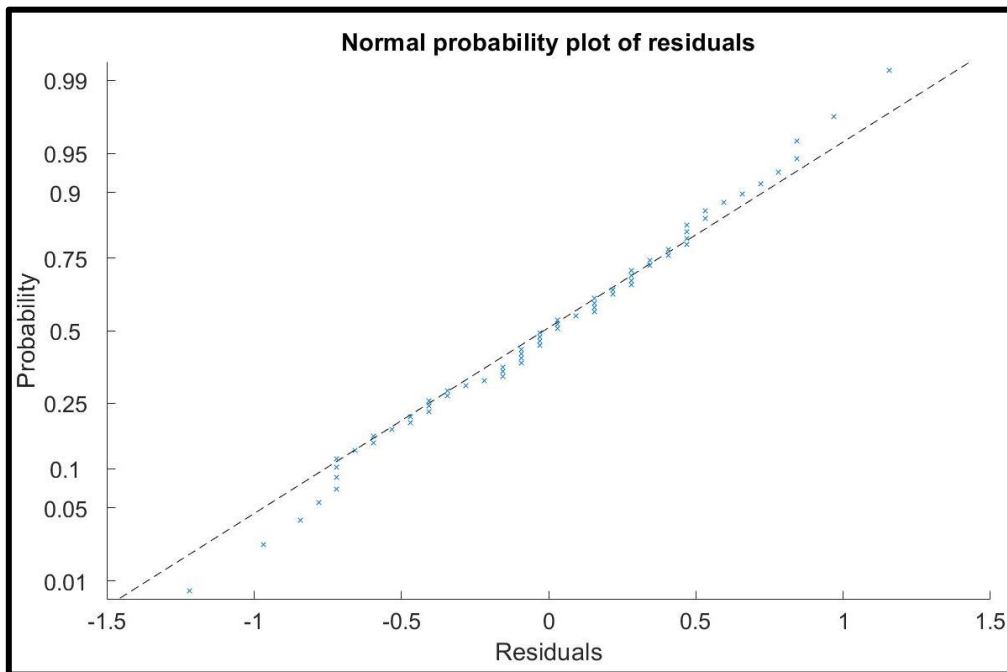


Figure 19: Normal probability plot of residuals for the edge quality regression of cube samples.

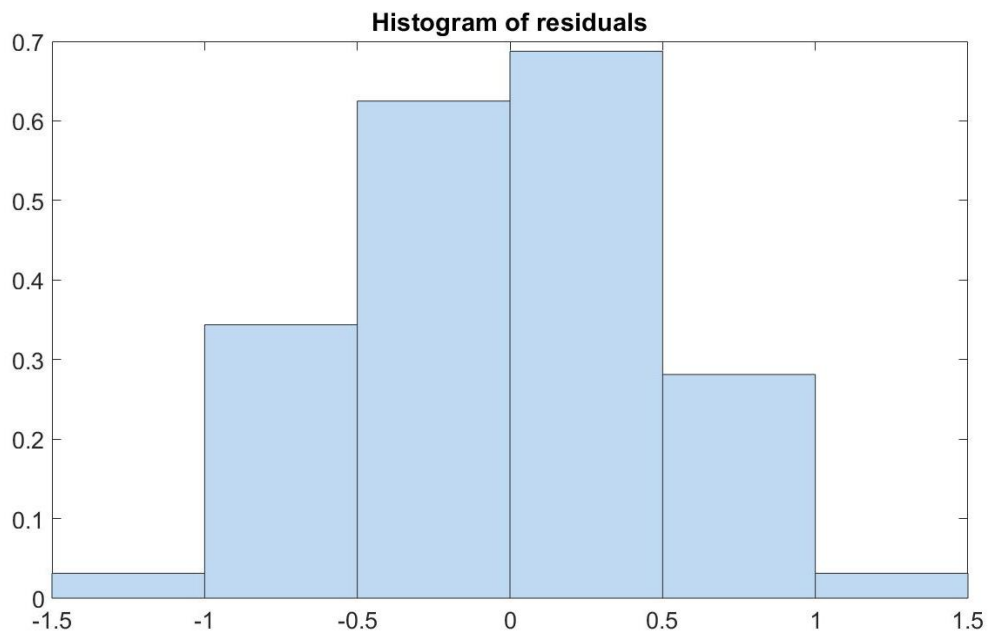


Figure 20: Histogram of residuals for the edge quality regression of cube samples.

The interaction between the model parameters is depicted in Figure 21.

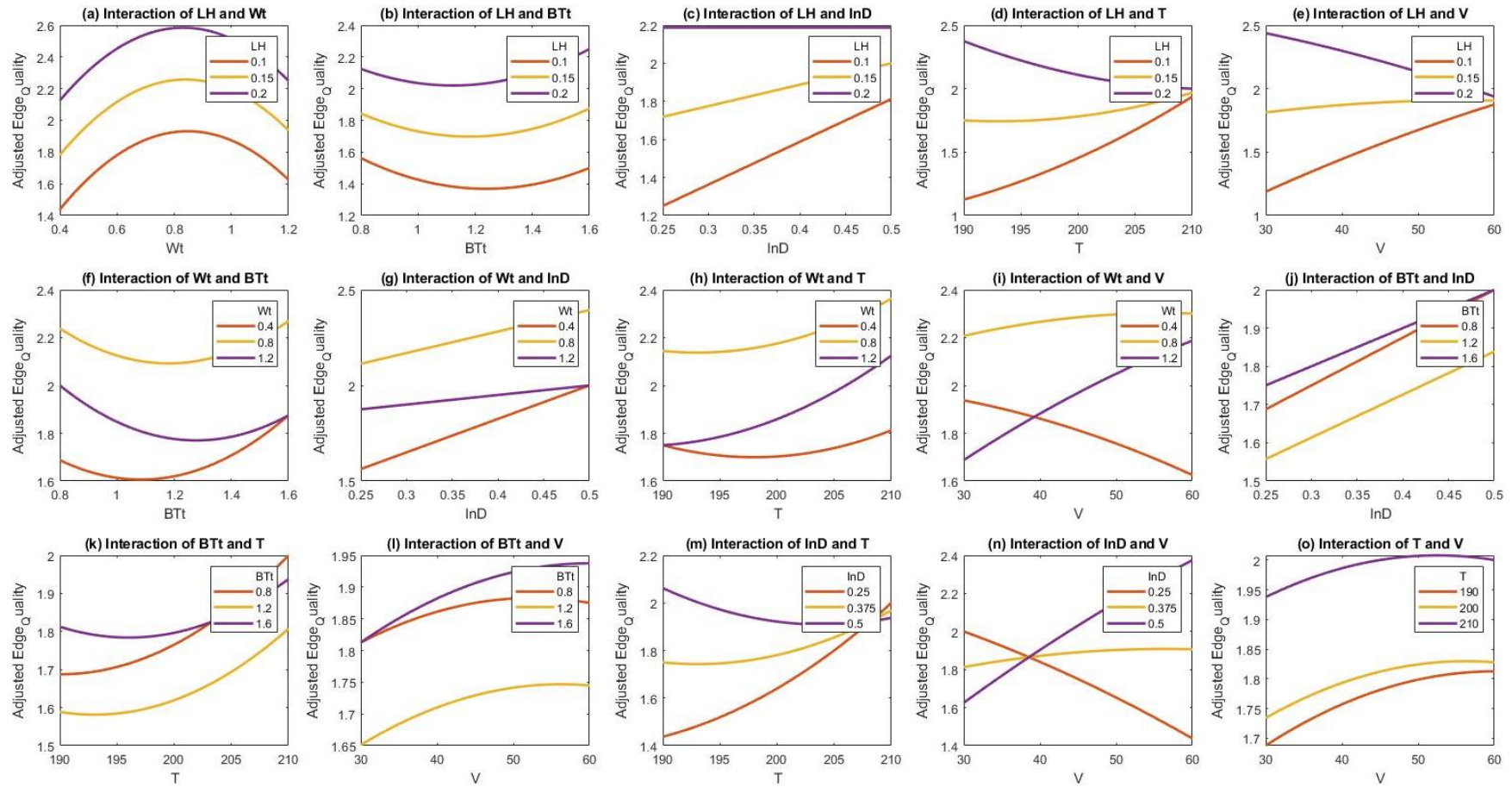


Figure 21: Parameters' interactions of the edge quality regression of cube samples: (a)  $LH$  and  $Wt$ , (b)  $LH$  and  $BTt$ , (c)  $LH$  and  $InD$ , (d)  $LH$  and  $T$ , (e)  $LH$  and  $V$ , (f)  $Wt$  and  $BTt$ , (g)  $Wt$  and  $InD$ , (h)  $Wt$  and  $T$ , (i)  $Wt$  and  $V$ , (j)  $BTt$  and  $InD$ , (k)  $BTt$  and  $T$ , (l)  $BTt$  and  $V$ , (m)  $InD$  and  $T$ , (n)  $InD$  and  $V$  and (o)  $T$  and  $V$ .

Last, the regression model of the surface quality output is given by (6) as follow:

$$\begin{aligned}
 \text{Surface Quality}_{cube} &= 3.453 + 0.5468Wt_n - 0.3593LH_nInD_n - 0.3281V_n \\
 &- 0.2968LH_n + 0.2656T_nV_n - 0.1718BTt_n \\
 &- 0.1406LH_nT_n - 0.1406InD_nT_n + 0.1406Wt_nV_n \\
 &- 0.1093Wt_nT_n - 0.1093InD_n + 0.1093Wt_nInD_n \\
 &- 0.0781LH_nV_n - 0.0781T_n
 \end{aligned} \tag{6}$$

The obtained R-Square value is 71% and a *p-value* of  $6.24 \times 10^{-6}$ . The ANOVA analysis shows that the wall thickness  $Wt_n$ , the interaction between layer height  $LH_n$  and infill density  $InD_n$  and the printing speed  $V_n$  are the most influential parameters on the surface quality output, in addition to the layer height  $LH_n$  as shown in Table 6.

Table 6: ANOVA table of surface quality of cube samples.

	Estimates	SE	t-stat	<i>p-value</i>
Intercept	3.453125	0.090533	38.14234	1.04E-30
$Wt_n$	0.546875	0.090533	6.040642	6.13E-07
$LH_n: InD_n$	-0.35938	0.090533	-3.96957	0.000329
$V_n$	-0.32813	0.090533	-3.62439	0.000888
$LH_n$	-0.29688	0.090533	-3.27921	0.002314
$T_n: V_n$	0.265625	0.090533	2.934026	0.005791
$BTt_n$	-0.17188	0.090533	-1.89849	0.065671
$LH_n: T_n$	-0.14063	0.090533	-1.55331	0.129098
$InD_n: T_n$	-0.14063	0.090533	-1.55331	0.129098
$Wt_n: V_n$	0.140625	0.090533	1.553308	0.129098
$Wt_n: T_n$	-0.10938	0.090533	-1.20813	0.234874
$InD_n$	-0.10938	0.090533	-1.20813	0.234874
$Wt_n: InD_n$	0.109375	0.090533	1.208128	0.234874
$LH_n: V_n$	-0.07813	0.090533	-0.86295	0.393878
$T_n$	-0.07812	0.090533	-0.86295	0.393878

In addition, the normal probability plot and histogram plot of residuals of the edge quality regression of the cube samples are graphed in Figure 22 and Figure 23. Fruitfully, the graphs show that the data are in good fit with model.

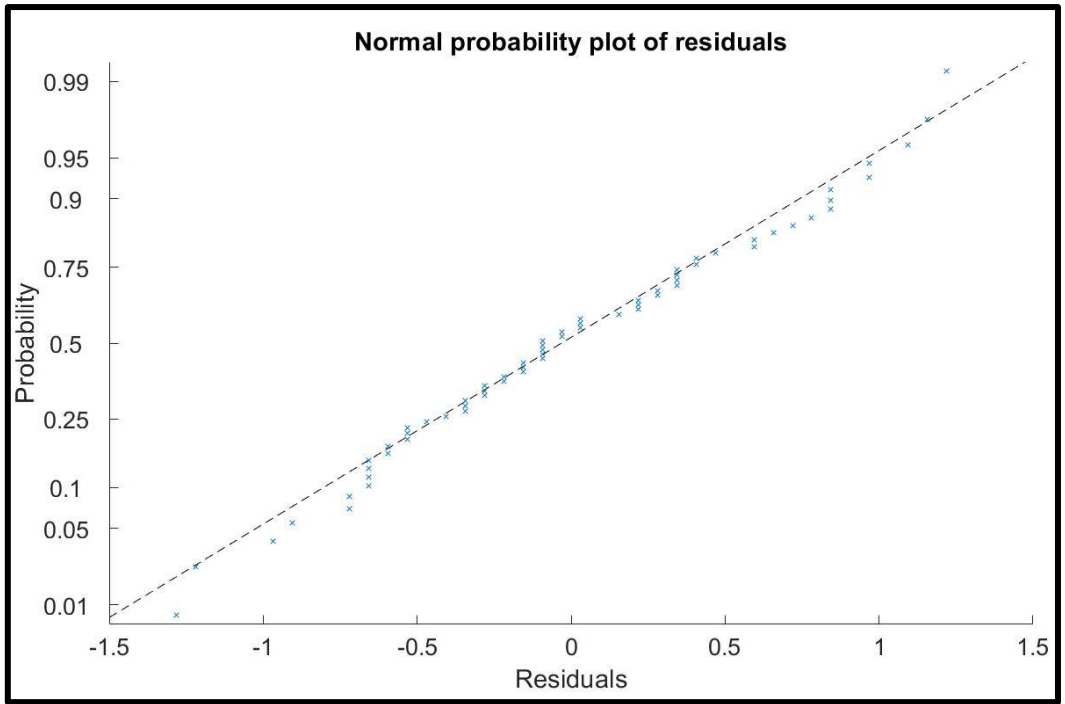


Figure 22: Normal probability plot of residuals for the surface quality regression of cube samples.

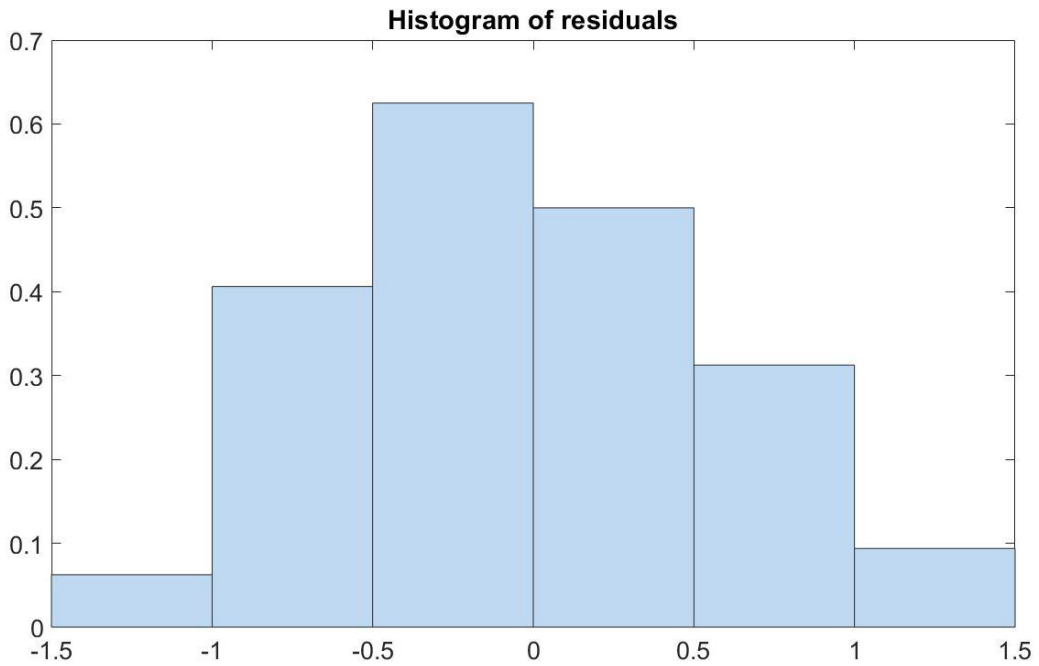


Figure 23: Histogram of residuals for the surface quality regression of cube samples.



Finally, the interaction between the model parameters for the edge quality output is illustrated in Figure 24.

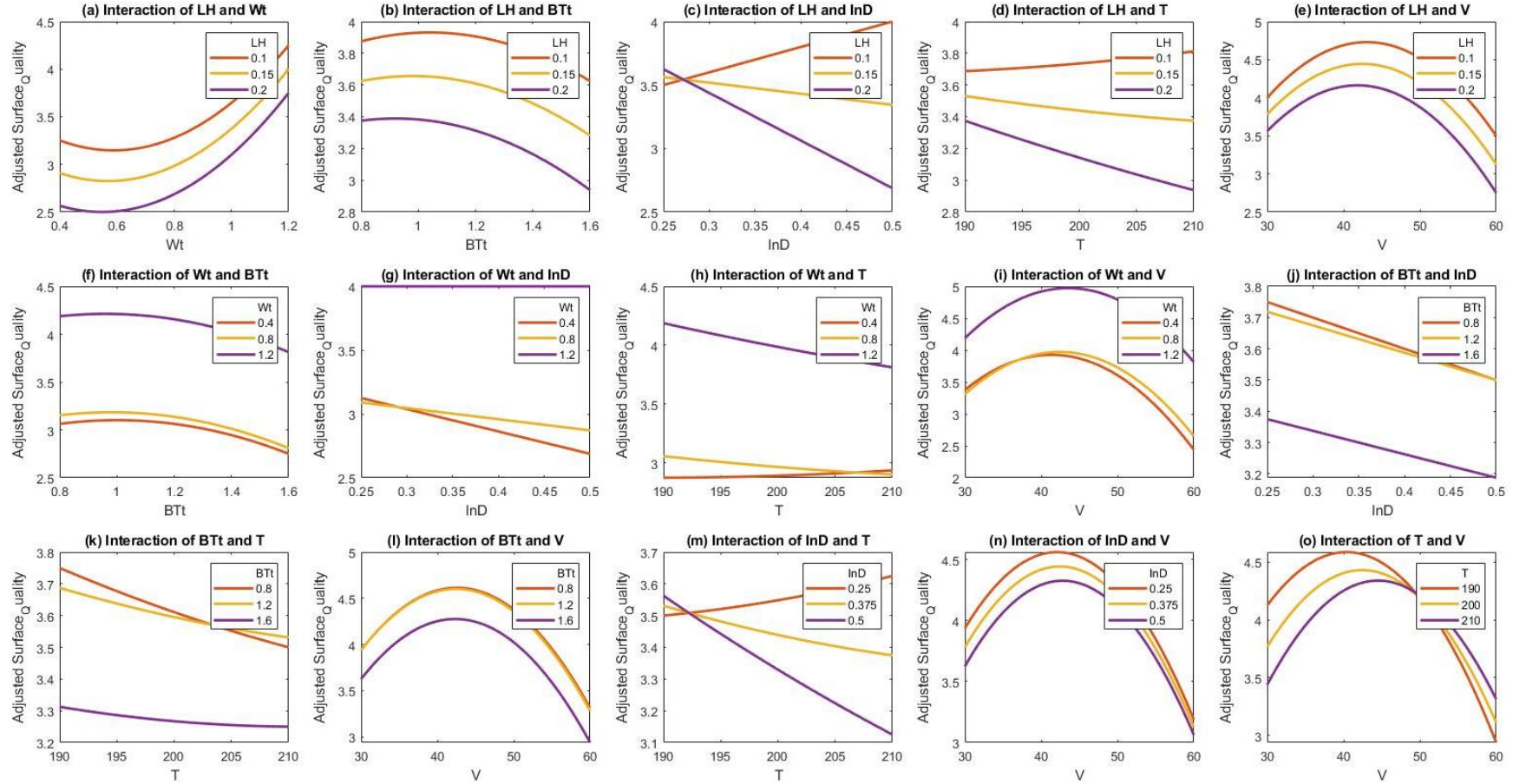


Figure 24: Parameters' interactions of the surface quality regression of cube samples: (a)  $LH$  and  $Wt$ , (b)  $LH$  and  $BTt$ , (c)  $LH$  and  $lnD$ , (d)  $LH$  and  $T$ , (e)  $LH$  and  $V$ , (f)  $Wt$  and  $BTt$ , (g)  $Wt$  and  $lnD$ , (h)  $Wt$  and  $T$ , (i)  $Wt$  and  $V$ , (j)  $BTt$  and  $lnD$ , (k)  $BTt$  and  $T$ , (l)  $BTt$  and  $V$ , (m)  $lnD$  and  $T$ , (n)  $lnD$  and  $V$  and (o)  $T$  and  $V$ .

### 4.3.2. CYLINDER MODEL ANALYSIS

Similarly, the same procedure considered in the cube model is followed. The main effects plots of the parameters on the three outputs are shown in Figure 25, Figure 26 and Figure 27.

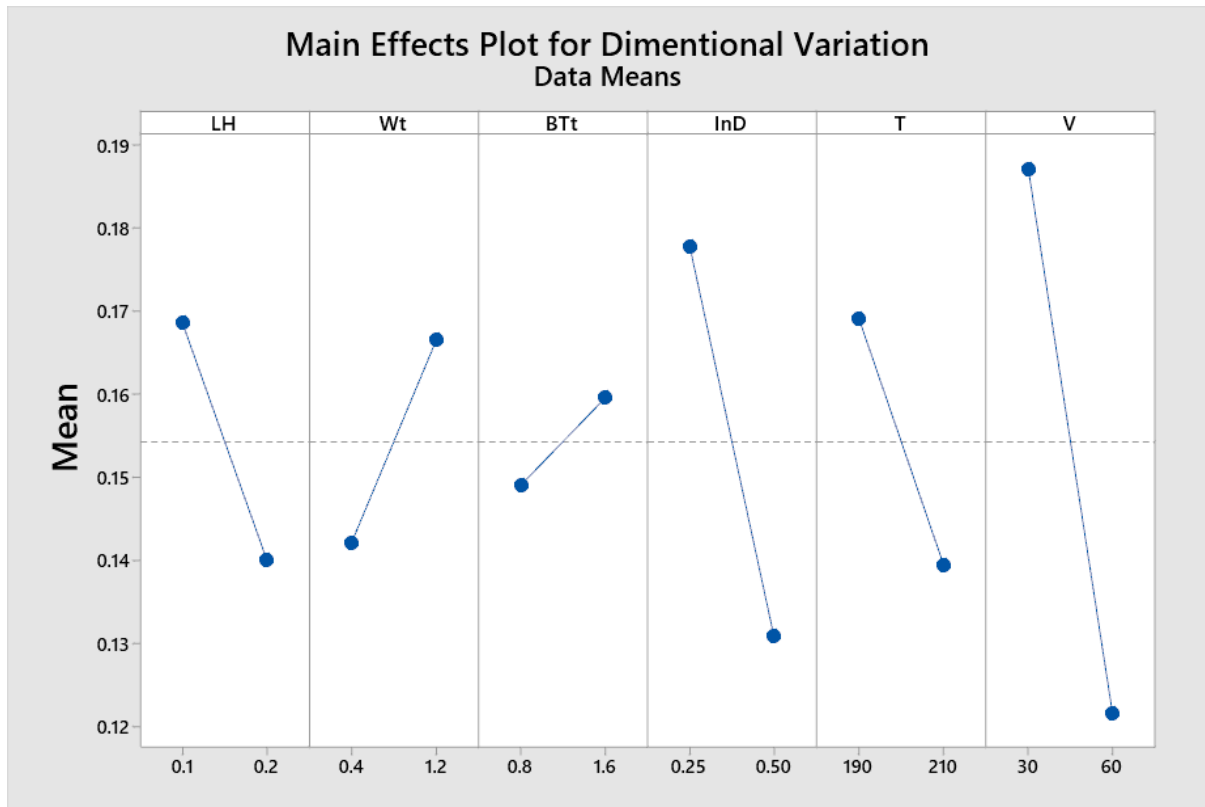


Figure 25: Main effects plot for dimensional variation of cylinder samples.

Obviously, all the three outputs are affected greatly by three or more parameters. This can be explained as the multi-axis movement of the printer head with a certain speed to create a single layer is crucial. Moreover, the infill connection with the walls of the printed samples is considered additional reason. Almost all parameters except the bottom/top thickness  $BTt$  and the temperature  $T$  are significant to the main outputs.

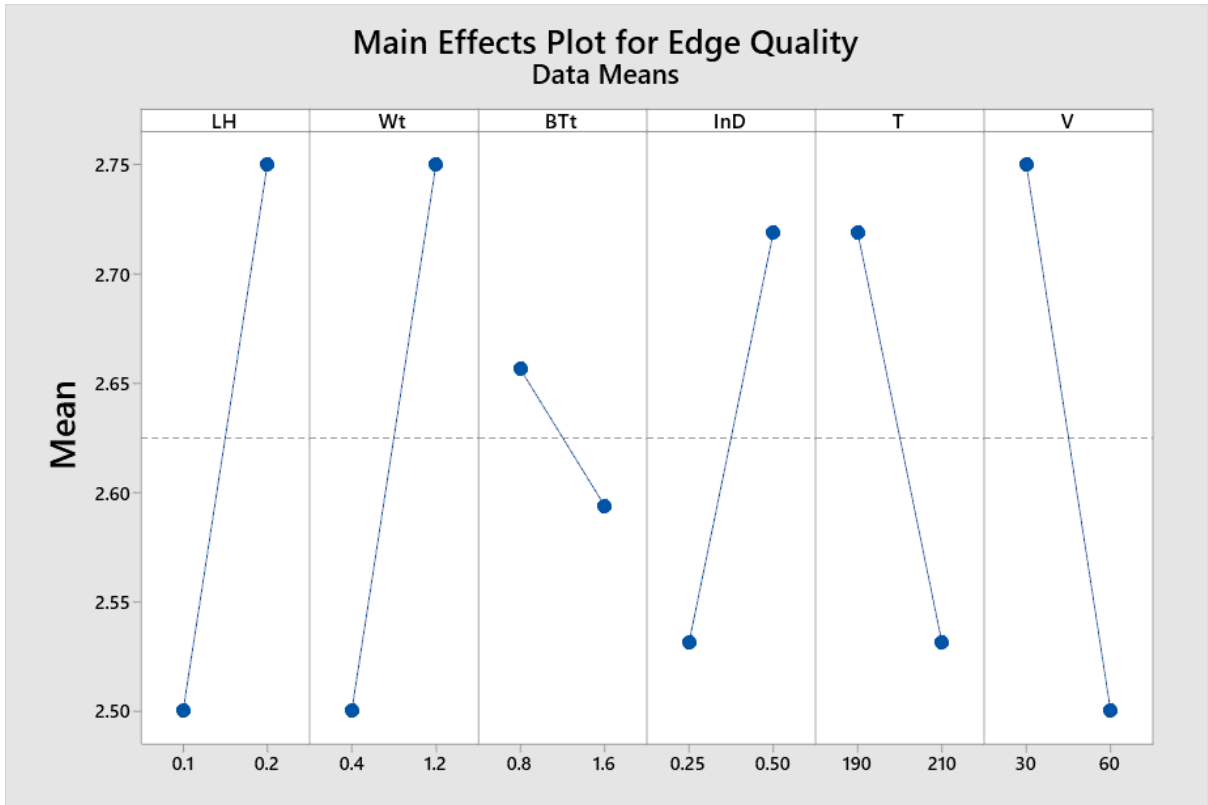


Figure 26: Main effects plot for edge quality of cylinder samples.

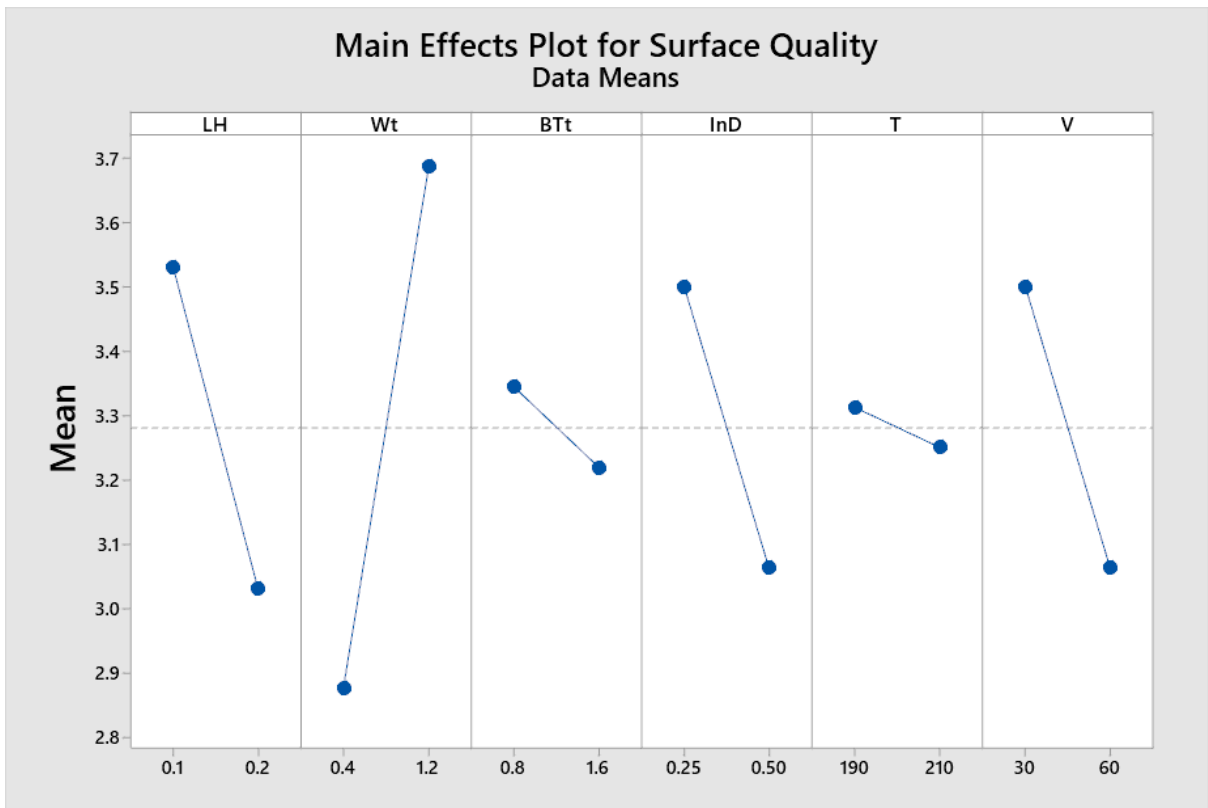


Figure 27: Main effects plot for surface quality of cylinder samples.

Moving forward to the quadratic regression of the cylinder model, the first model is the dimensional variation regression with normalized parameters, see Equation (7). The regression R-Square is 69.8% and the  $p$ -value is  $6.19 \times 10^{-5}$ . Then, the ANOVA analysis is carried out and shown in Table 7.

$$\begin{aligned}
 DV_{cylinder} = & 0.1542 - 0.0327V_n - 0.0234InD_n - 0.0188Wt_nV_n \\
 & - 0.01486T_n - 0.01486LH_n + 0.0122Wt_n \\
 & - 0.0107InD_nV_n + 0.0086LH_nT_n + 0.0058LH_nV_n \\
 & - 0.0056Wt_nT_n + 0.0052BTt_n - 0.0048BTt_nInD_n
 \end{aligned} \tag{7}$$

Table 7: ANOVA table of dimensional variation of cylinder samples.

	Estimates	SE	t-stat	$p$ -value
Intercept	0.154267	0.005867	26.2949	4.29E-25
$V_n$	-0.03279	0.005867	-5.5895	2.46E-06
$InD_n$	-0.02349	0.005867	-4.0035	0.000298
$Wt_n: V_n$	-0.01883	0.005867	-3.20901	0.002799
$T_n$	-0.01486	0.005867	-2.53214	0.015842
$LH_n$	-0.01424	0.005867	-2.4271	0.020352
$Wt_n$	0.012217	0.005867	2.082449	0.044468
$InD_n: V_n$	-0.01076	0.005867	-1.83471	0.074823
$LH_n: T_n$	0.008609	0.005867	1.467341	0.150966
$LH_n: V_n$	0.005849	0.005867	0.997028	0.325406
$Wt_n: T_n$	-0.00559	0.005867	-0.95298	0.346955
$BTt_n$	0.005241	0.005867	0.893333	0.377612
$BTt_n: InD_n$	-0.00483	0.005867	-0.82398	0.415375

In this case, the first 6 terms, excluding the constant term, in Table 7 are the most significant terms in the regression model of the cylinders' dimensional variation. The range of  $p$ -value for the mentioned parameters varies between  $[2.46 \times 10^{-6} \ 0.044468]$ . Furthermore, the normal probability and histogram plots of residuals is obtained to check the fitness of the model with

the data as show in Figure 28 and Figure 29, respectively. Fortunately, the graphs indicate a good fit of the data.

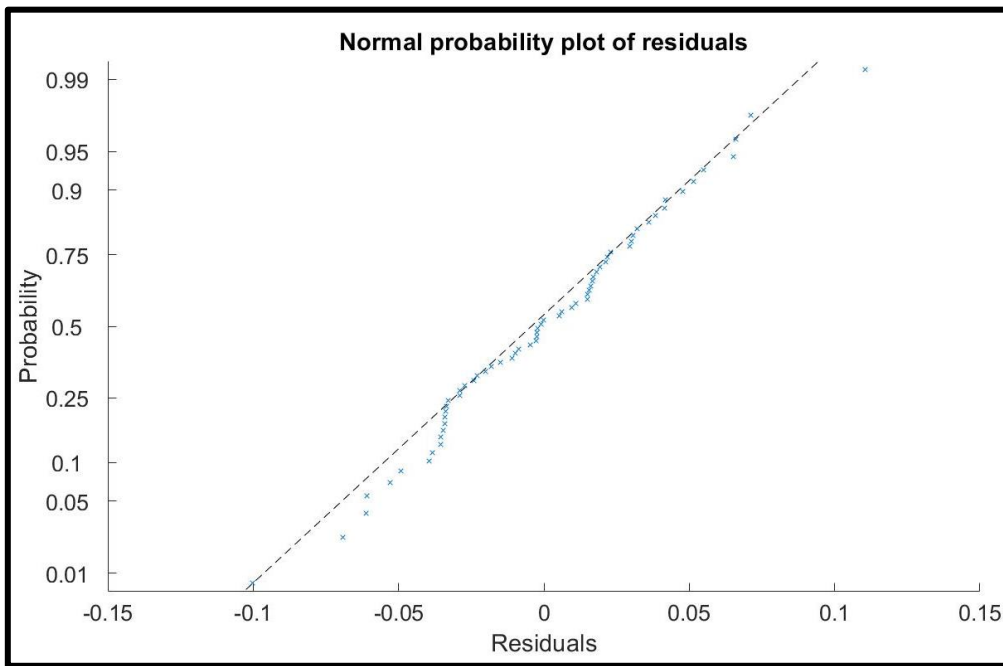


Figure 28: Normal probability plot of residuals for the dimensional variation regression of cylinder samples.

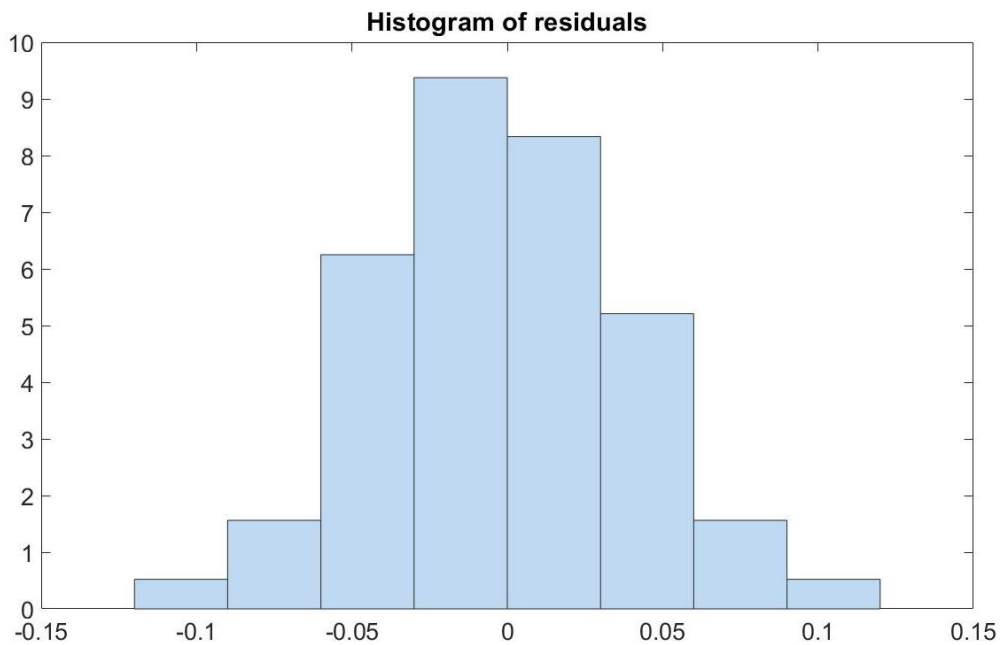


Figure 29: Histogram of residuals for the dimensional variation regression of cylinder samples.

Similarly, the interactions between the model parameters are shown in Figure 30. Only the interaction between  $Wt$  and  $V$  and the interaction between  $BTt$  and  $InD$  are found significant.

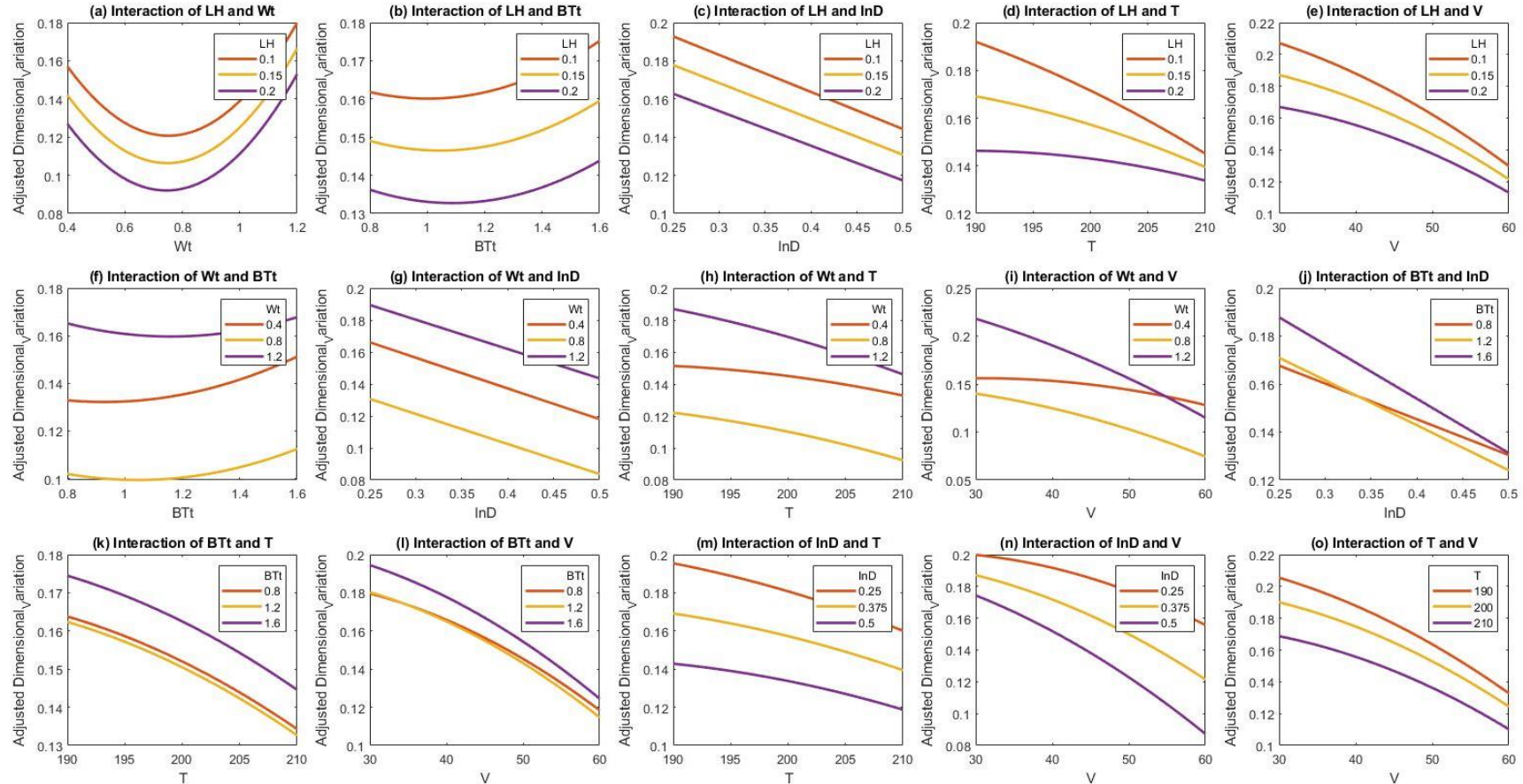


Figure 30: Parameters' interactions of the dimensional variation regression of cylinder samples: (a)  $LH$  and  $Wt$ , (b)  $LH$  and  $BTt$ , (c)  $LH$  and  $InD$ , (d)  $LH$  and  $T$ , (e)  $LH$  and  $V$ , (f)  $Wt$  and  $BTt$ , (g)  $Wt$  and  $InD$ , (h)  $Wt$  and  $T$ , (i)  $Wt$  and  $V$ , (j)  $BTt$  and  $InD$ , (k)  $BTt$  and  $T$ , (l)  $BTt$  and  $V$ , (m)  $InD$  and  $T$ , (n)  $InD$  and  $V$  and (o)  $T$  and  $V$ .

The second model is the edge quality of cylinder samples, see Equation (8). The R-Squared value of this model is 64.5%, and the  $p$ -value is 0.00728. The model terms show close significance as shown in the ANOVA analysis in Table 8. The normal probability plot and histogram plot of the residuals are show in Figure 31 and Figure 32, respectively. Unfortunately, the graphs show slight lack of fit of the data, however, the model is acceptable for the given design of experiment as the parameters' levels are limited to 2 level full-factorial design.

$$\begin{aligned}
 \text{Edge Quality}_{\text{cylinder}} &= 2.625 - 0.15625LH_n InD_n + 0.15625LH_n V_n \\
 &+ 0.125LH_n - 0.125BTt_n InD_n - 0.125BTt_n T_n \\
 &+ 0.125Wt_n - 0.125LH_n Wt_n - 0.125V_n + 0.0937InD_n \\
 &- 0.0973LH_n BTt_n - 0.0937T_n - 0.0625Wt_n V_n
 \end{aligned} \tag{8}$$

Table 8: ANOVA table of edge quality of cylinder samples.

	Estimates	SE	t-stat	$p$ -value
Intercept	2.625	0.059449358	44.15522858	5.96E-33
$LH_n: InD_n$	-0.15625	0.059449358	-2.6282874	0.012535853
$InD_n: V_n$	1.56E-01	0.059449358	2.63E+00	0.012535853
$LH_n$	0.125	0.059449358	2.102629932	0.042554919
$BTt_n: InD_n$	-0.125	0.059449358	-2.1026299	0.042554919
$BTt_n: T_n$	-0.125	0.059449358	-2.1026299	0.042554919
$Wt_n$	0.125	0.059449358	2.102629932	0.042554919
$LH_n: Wt_n$	-0.125	0.059449358	-2.1026299	0.042554919
$V_n$	-0.125	0.059449358	-2.1026299	0.042554919
$InD_n$	0.09375	0.059449358	1.576972449	0.123549948
$LH_n: BTt_n$	-0.09375	0.059449358	-1.5769724	0.123549948
$T_n$	-0.09375	0.059449358	-1.5769724	0.123549948
$Wt_n: V_n$	-0.0625	0.059449358	-1.0513149	0.3001201

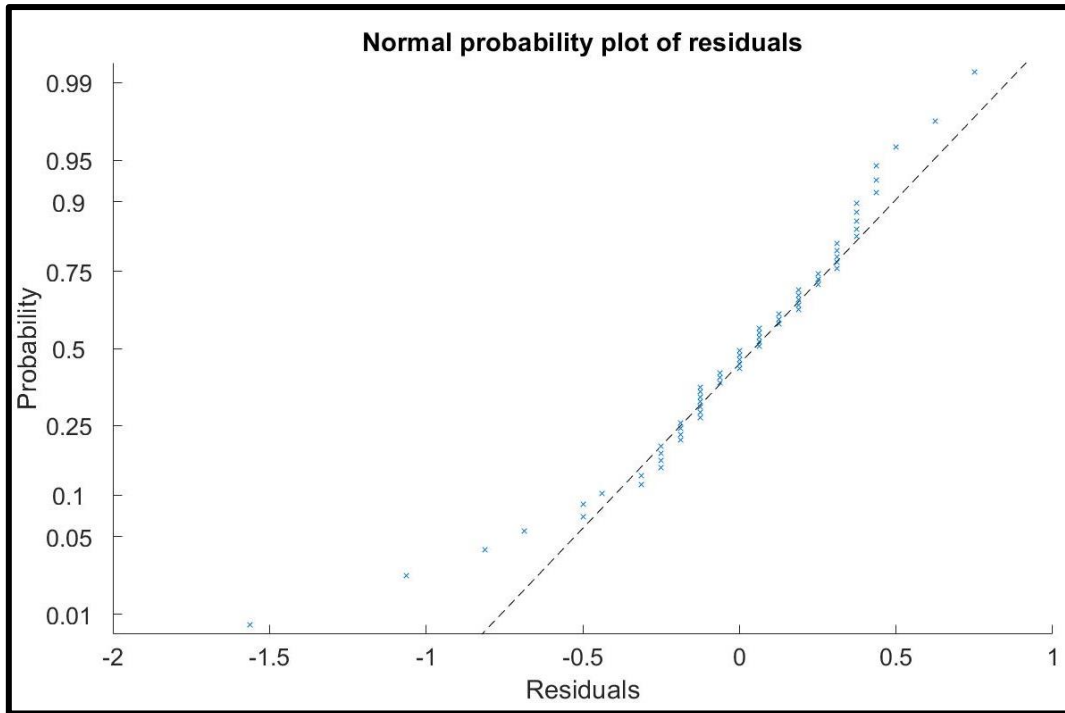


Figure 31: Normal probability plot of residuals for the edge quality regression of cylinder samples.

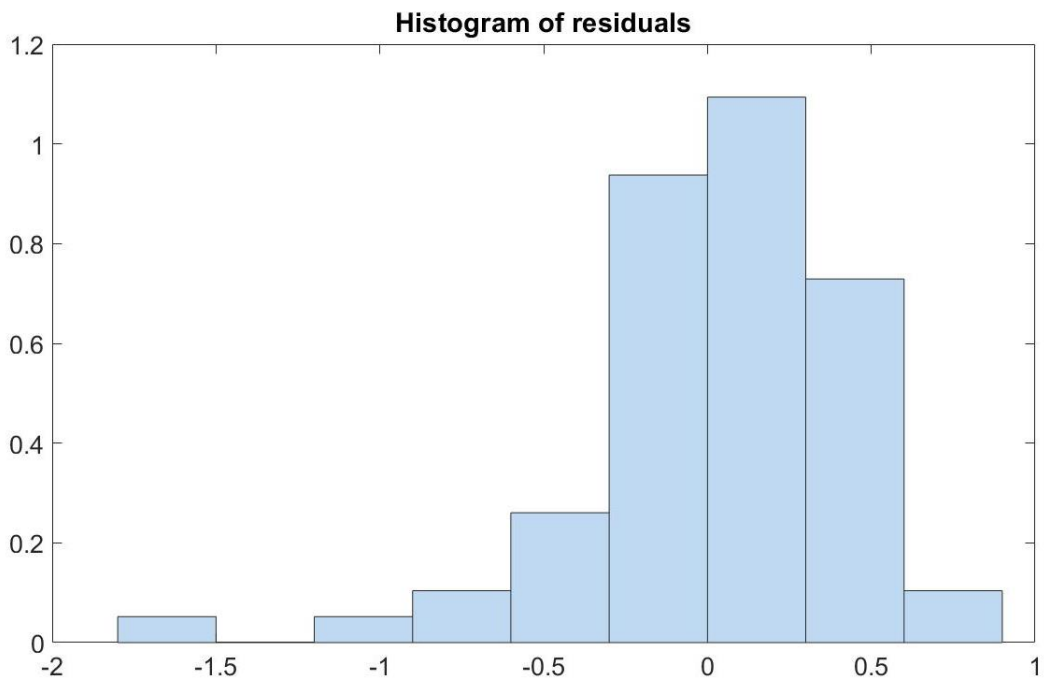


Figure 32: Histogram of residuals for the edge quality regression of cylinder samples.



Last, the interactions between model parameters for the edge quality regression is illustrated in Figure 29.

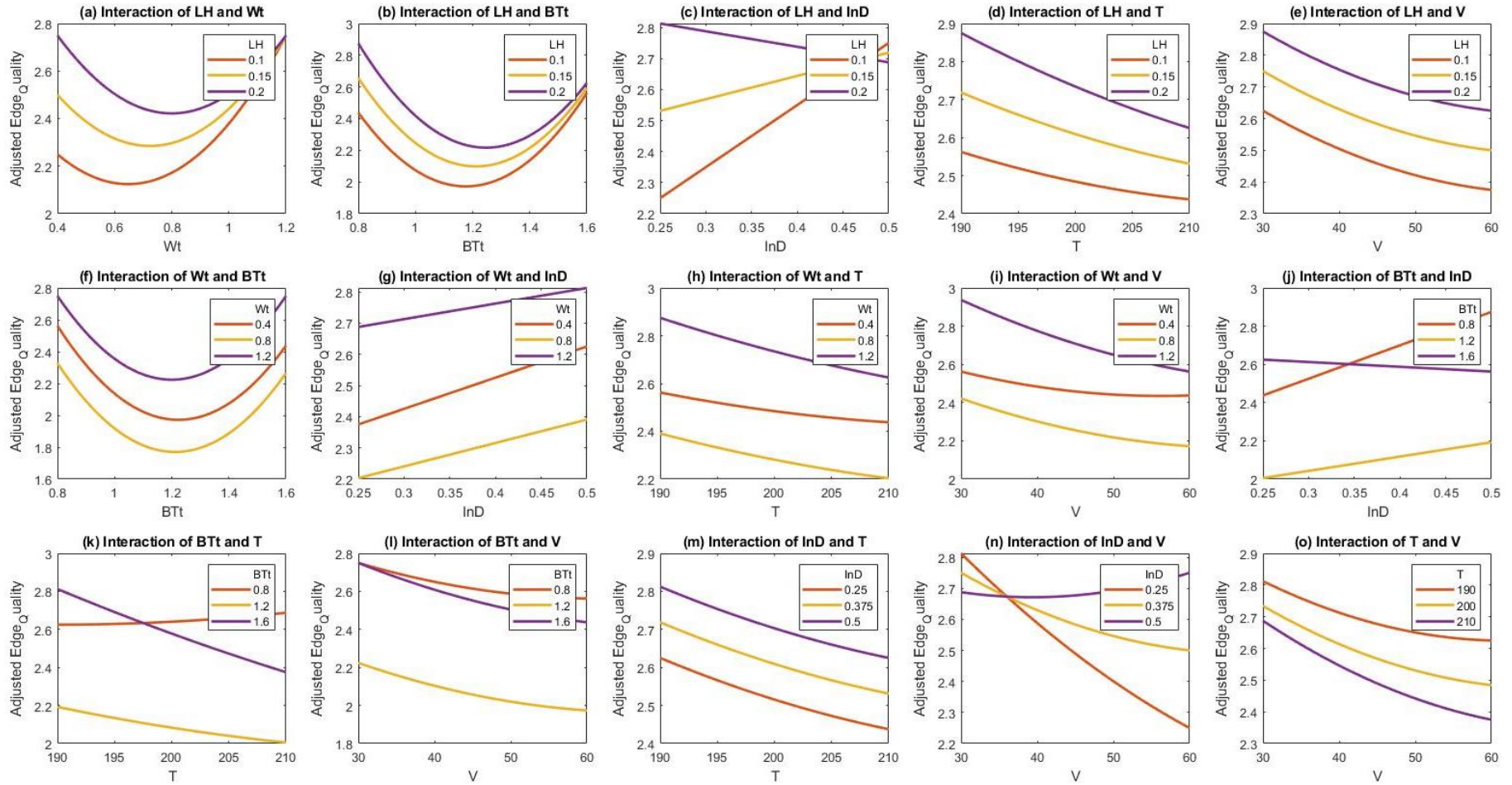


Figure 33: Parameters' interactions of the edge quality regression of cylinder samples: (a) *LH* and *Wt*, (b) *LH* and *BTt*, (c) *LH* and *InD*, (d) *LH* and *T*, (e) *LH* and *V*, (f) *Wt* and *BTt*, (g) *Wt* and *InD*, (h) *Wt* and *T*, (i) *Wt* and *V*, (j) *BTt* and *InD*, (k) *BTt* and *T*, (l) *BTt* and *V*, (m) *InD* and *T*, (n) *InD* and *V* and (o) *T* and *V*.

The last regression model in this study is the surface quality of cylinder samples. The obtained R-Squared value is 65.5%, and the *p-value* is 0.000115. The model is presented in Equation (9). To wrap up this analysis, the ANOVA analysis is presented in Table 9. Furthermore, the normal probability plot and histogram plot of the residuals show a good fit of the data as shown in Figure 34 and Figure 35, respectively.

$$\begin{aligned}
 & \text{Surface Quality}_{cylinder} \\
 & = 3.2812 + 0.4062Wt_n - 0.25LH_n + 0.2187T_nV_n \\
 & \quad - 0.2187InD_n - 0.2187V_n + 0.125LH_nWt_n \\
 & \quad - 0.125LH_nInD_n + 0.125LH_nV_n - 0.0937Wt_nInD_n \\
 & \quad - 0.0937LH_nBTt_n + 0.0937InD_nT_n - 0.0625Wt_nBTt_n \\
 & \quad - 0.0625BTt_n
 \end{aligned} \tag{9}$$

Table 9: ANOVA table of surface quality of cylinder samples.

	Estimates	SE	t-stat	p-value
Intercept	3.28125	0.075937	43.21038	1.28E-32
$Wt_n$	0.40625	0.075937	5.349857	5.13981E-06
$LH_n$	-0.25	0.075937	-3.29222	0.002233397
$T_n: V_n$	0.21875	0.075937	2.880692	0.006645893
$InD_n$	-0.21875	0.075937	-2.88069	0.006645893
$V_n$	-0.21875	0.075937	-2.88069	0.006645893
$LH_n: Wt_n$	0.125	0.075937	1.64611	0.108445186
$LH_n: InD_n$	-1.25E-01	0.075937	-1.65E+00	0.108445186
$LH_n: V_n$	0.125	0.075937	1.64611	0.108445186
$Wt_n: InD_n$	-0.09375	0.075937	-1.23458	0.224984068
$LH_n: BTt_n$	-0.09375	0.075937	-1.23458	0.224984068
$InD_n: T_n$	0.09375	0.075937	1.234582	0.224984068
$Wt_n: BTt_n$	-0.0625	0.075937	-0.82305	0.415895769
$BTt_n$	-0.0625	0.075937	-0.82305	0.415895769

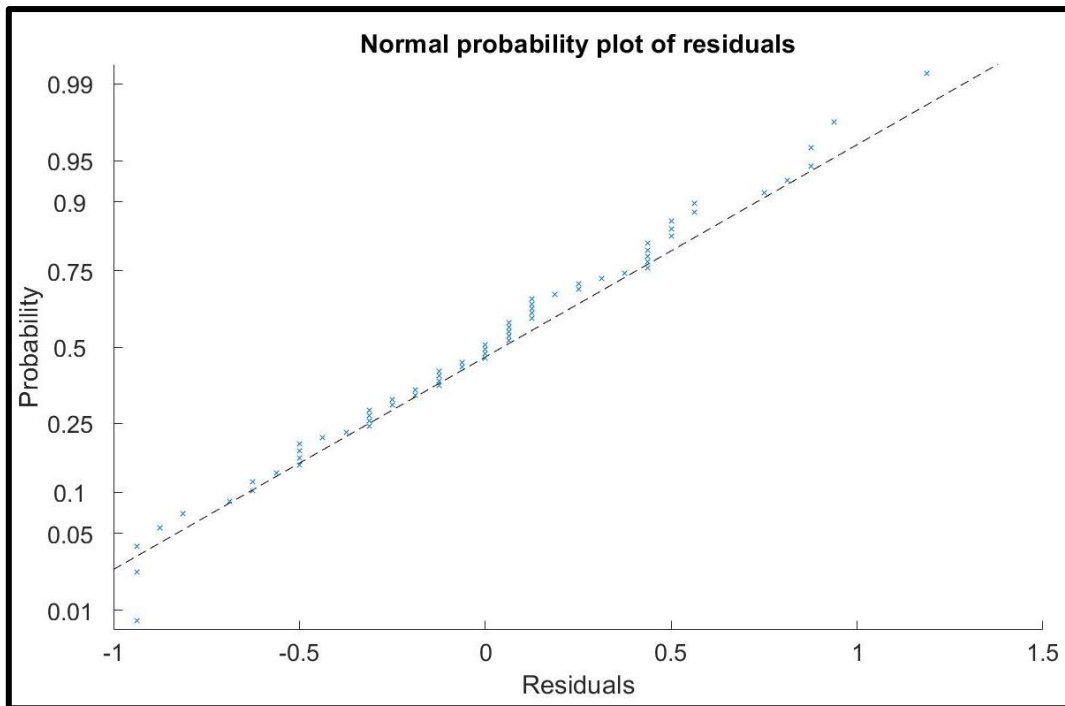


Figure 34: Normal probability plot of residuals for the surface quality regression of cylinder samples.

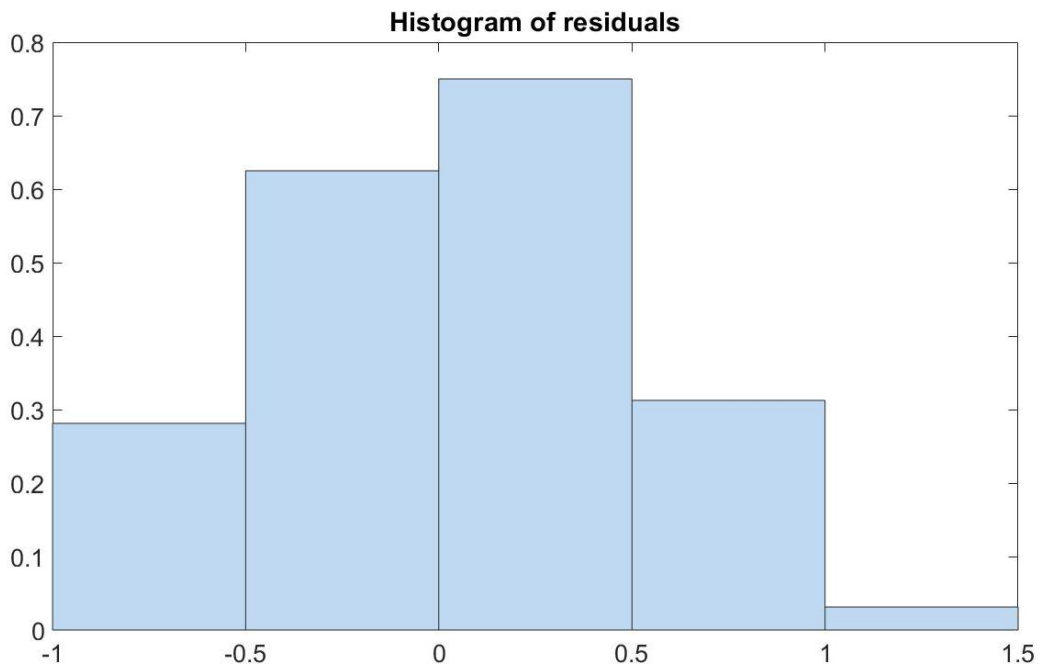


Figure 35: Histogram of residuals for the surface quality regression of cylinder samples.

Finally, the interaction between parameters for the surface quality regression model is depicted in Figure 36.

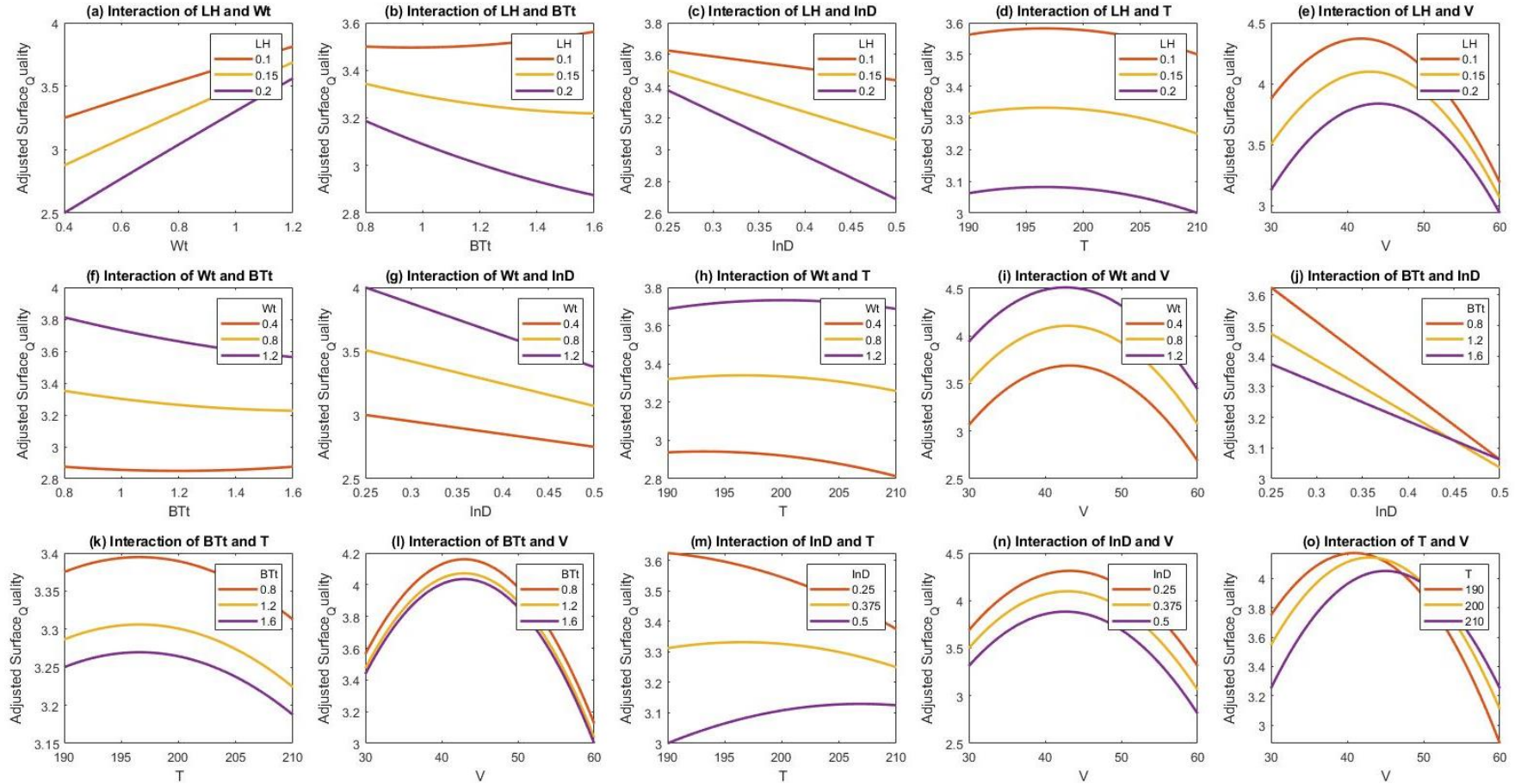


Figure 36: Parameters' interactions of the surface quality regression of cylinder samples: (a) *LH* and *Wt*, (b) *LH* and *BTt*, (c) *LH* and *InD*, (d) *LH* and *T*, (e) *LH* and *V*, (f) *Wt* and *BTt*, (g) *Wt* and *InD*, (h) *Wt* and *T*, (i) *Wt* and *V*, (j) *BTt* and *InD*, (k) *BTt* and *T*, (l) *BTt* and *V*, (m) *InD* and *T*, (n) *InD* and *V* and (o) *T* and *V*.

## 4.4. Multi-Objective Optimization

In this section, the obtained regression models from the ANOVA analysis are optimized using multi-objective optimization techniques on MATLAB 9.10 2021a. The used techniques in this study are multi-objective genetic algorithm (MOGA) and multi-objective pareto search algorithm (MOPSA). Although, the study includes two different geometries; cube and cylinder, hence, the optimization study is carried out separately. The aim of this research is to optimize three different outputs in the process of 3D printing by fused deposition modelling (FDM). The objectives are the dimensional accuracy, edge quality and surface quality. First, the cube model mentioned in section 4.3.1 presents the three desired objective functions (4)-(6). However, the objective of the model is to minimize the dimensional variation (4) and to maximize the edge quality (5) and the surface quality (6). Meanwhile, MATLAB optimization functions search for the minimal values of the input objective, hence, the multiplicative inverse of (5) and (6) is considered the second and the third objectives. The upper and lower bounds of the model parameters are common between cube and cylinder models. The developed multi-objective optimization model is shown in Table 10.

Table 10: Optimization model of cube samples.

Item	
<b>No. of variables</b>	6
<b>Variables</b>	$LH, Wt, BTt, InD, T, V$
<b>Objectives</b>	$\min(DV_{cube})$
	$\min\left(\frac{1}{Edge\ Quality_{cube}}\right)$
	$\min\left(\frac{1}{Surface\ Quality_{cube}}\right)$
<b>Lower bounds</b>	[0.1, 0.4, 0.8, 0.25, 190, 30]
<b>Upper bounds</b>	[0.2, 1.2, 1.6, 0.50, 210, 60]

For the MOGA simulation, the initial starting point is the average vector of the lower and upper bounds;  $x_0 = [0.15 \ 0.8 \ 1.2 \ 0.375 \ 200 \ 45]$ . The number of populations and the maximum generations are set to 500 and 2000, respectively. It is found that the pareto plot function is limited to visualize the algorithm search, in addition to the lack of a 2-D representation. Hence, the parallel plot function on MATLAB provides a sufficient visualization of the optimization output. In Figure 37, the results of the optimal solution scheme are provided, also, the optimal solution is marked in green. The optimal solution can be found in Table 11.

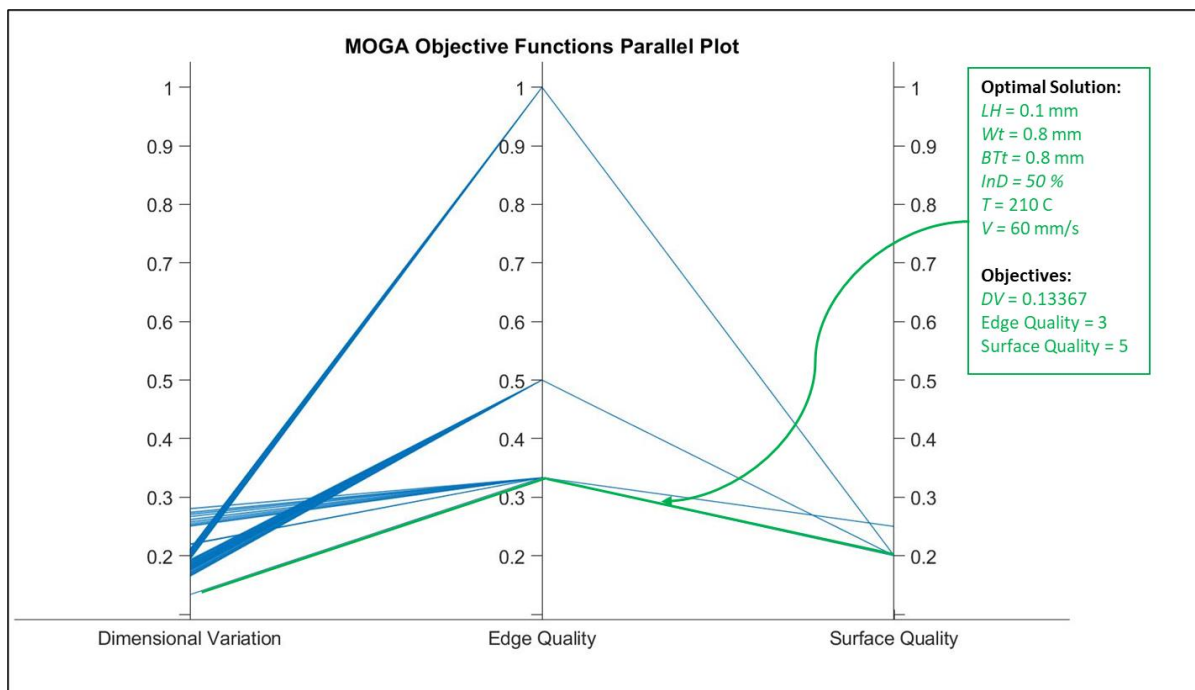


Figure 37: Parallel Plot of MOGA simulation for cube samples.

Table 11: MOGA optimal solution for cube samples.

Parameters						Results			Comp. Time
<i>LH</i>	<i>Wt</i>	<i>BTt</i>	<i>InD</i>	<i>T</i>	<i>V</i>	Dimensional Variation	Edge Quality	Surface Quality	(s)
(mm)	(mm)	(mm)	(%)	(°C)	(mm/s)				
0.1	0.8	0.8	50	210	60	0.13367	3	5	19.7



On the other hand, the MOPSA does not require initial starting point, however, the maximum iterations are set to be 10000. The MOPSA results are the same as the MOGA results for the cube samples except MOPSA is 28 times faster than MOGA in computational time. The parallel plot graph that is obtained from the results of MOPSA simulation is shown in Figure 38. Also, the optimal printing parameters of MOPSA are shown in Table 12.

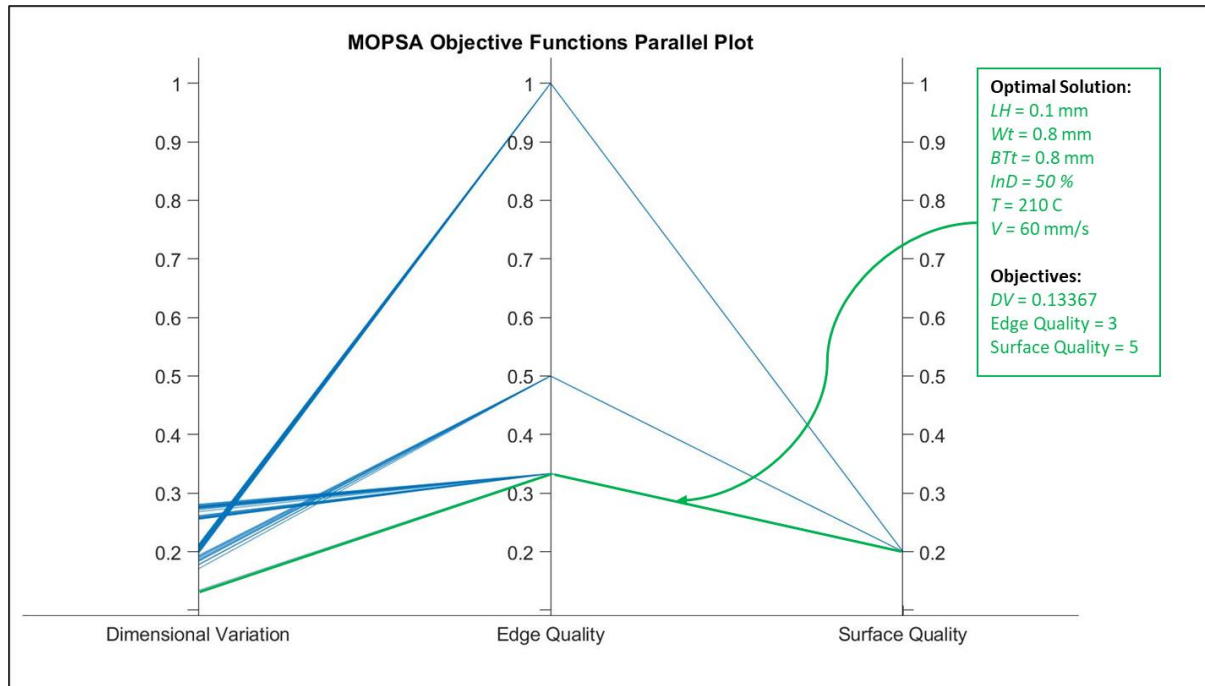


Figure 38: Parallel Plot of MOPSA simulation for cube samples.

Table 12: MOPSA optimal solution for cube samples.

Parameters						Results			Comp. Time
<i>LH</i>	<i>Wt</i>	<i>BTt</i>	<i>InD</i>	<i>T</i>	<i>V</i>	Dimensional	Edge	Surface	(s)
(mm)	(mm)	(mm)	(%)	(°C)	(mm/s)	Variation	Quality	Quality	
0.1	0.8	0.8	50	210	60	0.13367	3	5	0.72

In the other case of cylinder samples, the same procedure is considered. The optimization model is shown in Table 13. Moreover, the two optimization techniques are carried out with the same options mentioned in the cube case.

Table 13: Optimization model of cylinder samples.

Item	
<b>No. of variables</b>	6
<b>Variables</b>	$LH, Wt, BTt, InD, T, V$
<b>Objectives</b>	$\min(DV_{cylinder})$
	$\min\left(\frac{1}{Edge\ Quality_{cylinder}}\right)$
	$\min\left(\frac{1}{Surface\ Quality_{cylinder}}\right)$
<b>Lower bounds</b>	[0.1, 0.4, 0.8, 0.25, 190, 30]
<b>Upper bounds</b>	[0.2, 1.2, 1.6, 0.50, 210, 60]

The optimal printing parameters are different from the obtained parameters in the cube samples. In Figure 39, the optimal solution gives lower surface quality level at 4, while the edge quality level is 3, and the dimensional variation is 0.05951. The optimal parameters can be shown in Table 14.

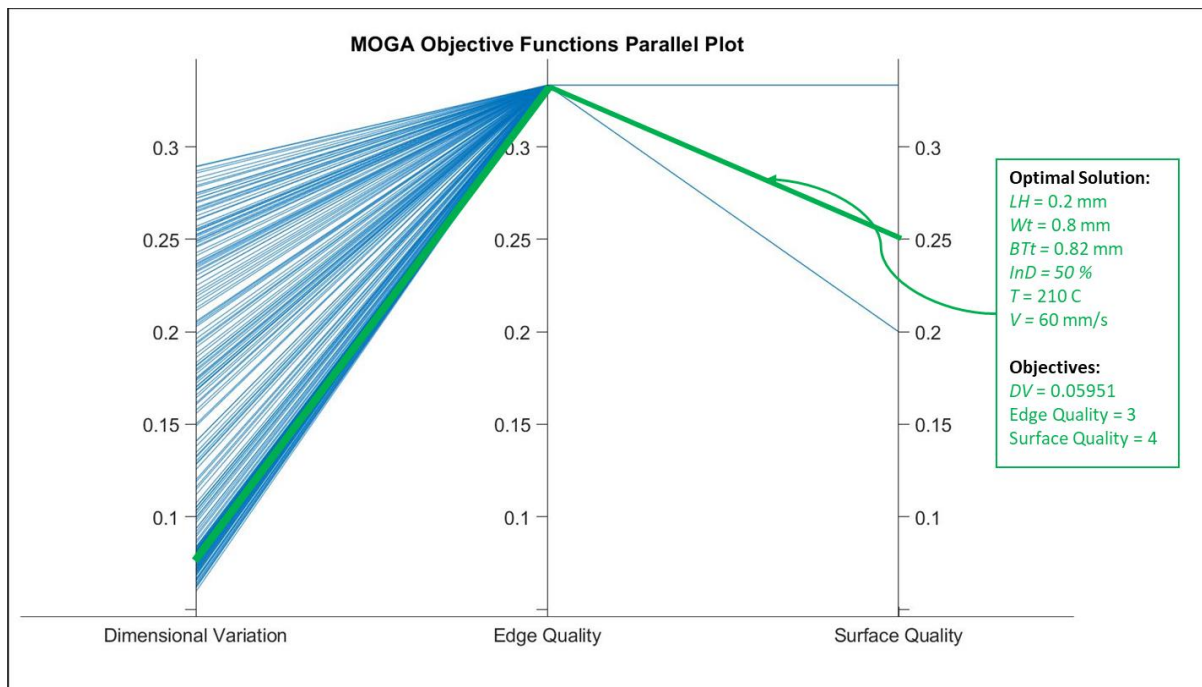


Figure 39: Parallel Plot of MOGA simulation for cylinder samples.



Table 14: MOGA optimal solution for cylinder samples.

Parameters						Results			Comp. Time
<i>LH</i> (mm)	<i>Wt</i> (mm)	<i>BTt</i> (mm)	<i>InD</i> (%)	<i>T</i> (°C)	<i>V</i> (mm/s)	Dimensional Variation	Edge Quality	Surface Quality	(s)
0.2	0.8	0.82	50	210	60	0.05951	3	4	23.5

The other technique MOPSA records different optimal solution with a slight effect on the objective as shown in Figure 40, however, the MOPSA remains faster than the MOGA technique. Finally, the optimal solution for cylinder samples using MOPSA technique is shown in Table 15.

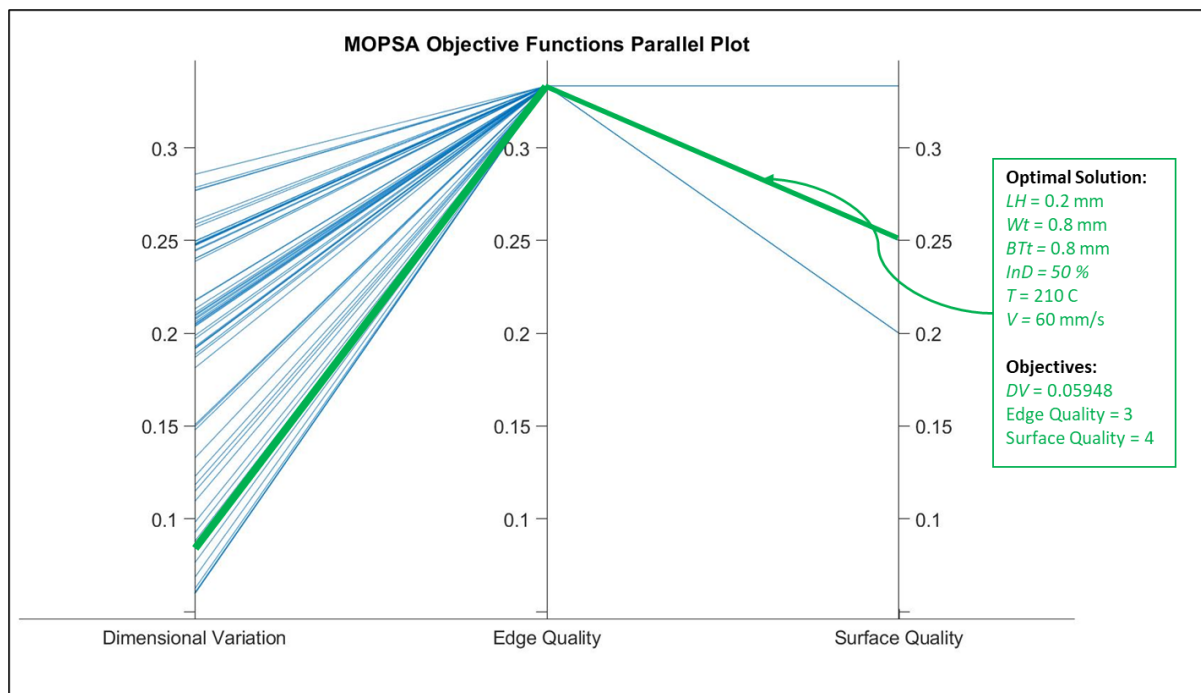


Figure 40: Parallel Plot of MOPSA simulation for cylinder samples.

Table 15: MOPSA optimal solution for cylinder samples.

Parameters						Results			Comp. Time
<i>LH</i> (mm)	<i>Wt</i> (mm)	<i>BTt</i> (mm)	<i>InD</i> (%)	<i>T</i> (°C)	<i>V</i> (mm/s)	Dimensional Variation	Edge Quality	Surface Quality	(s)
0.2	0.8	0.8	50	210	60	0.05948	3	4	0.86

## 4.5. Discussion

The FDM process is considered one of the most complicated and unpredictable additive manufacturing techniques. For many reasons, relating certain printing parameters to the final printed samples quality is challenging. First, the printer machine hardware related issues are unpredictable, for example, the motors vibrations and movement steps. No matter how motors are aligned and calibrated, there will be some negative effects on the printer performance and accuracy. Another reason, the printer structure stability can disturb the printing process. In addition, the printing parameters are enormously various which complicates the mathematical model development. These reasons are crucial to be mentioned as presented in this study, the lack of fit of the regression between printing parameters and final product quality is remarkable. In addition, the design of experiment that accommodates for full factorial design with 2-level and 6 factors tends to eliminate the nonlinearity of the parameters effect on the output. That's why all the polynomial terms of the second degree were removed from the presented models. However, involving as much as possible parameters in one model is one of this research priorities. Obviously, the influence of each single parameter on the final product's quality seems to be weak, however, the interactions between parameters attain higher levels of influence. Though, the optimization results are compared to find the optimal printing conditions for cubes and cylinders, see Table 16. The optimal solutions of both cases presented in this study are tested, see Figure 41. The cylinder part remains having a stair case issue on the surface; hence, the surface quality level is 4 as expected. The printed samples results are close to the model results, see Table 17. The dimensional variation relative errors between the printed samples and the optimized model are 11.6% and 13.48% for the cube and cylinder, respectively. Meanwhile, the edge quality and surface quality levels are matching the optimization model results.



Figure 41: Printed samples using the optimal parameters obtained in the study.

Finally, in the next chapter, the conclusions will be illustrated carefully. Furthermore, a deeper insight in the required future work will be presented.

Table 16: Comparison between different optimization techniques on cube and cylinder cases.

Case	Opt. Method	Parameters						Results			Comp. Time
		<i>LH</i> (mm)	<i>Wt</i> (mm)	<i>BTt</i> (mm)	<i>InD</i> (%)	<i>T</i> (°C)	<i>V</i> (mm/s)	Dimensional Variation	Edge Quality	Surface Quality	
Cube	MOGA	0.1	0.8	0.8	50	210	60	0.13367	3	5	19.7
	MOPSA	0.1	0.8	0.8	50	210	60	0.13367	3	5	0.72
Cylinder	MOGA	0.2	0.8	0.82	50	210	60	0.05951	3	4	23.5
	MOPSA	0.2	0.8	0.8	50	210	60	0.05948	3	4	0.86

Table 17: Comparison between printed samples with optimal parameters and the obtained model.

Case	Parameters						Dimensional	Error	Edge	Error	Surface	Error
	<i>LH</i> (mm)	<i>Wt</i> (mm)	<i>BTt</i> (mm)	<i>InD</i> (%)	<i>T</i> (°C)	<i>V</i> (mm/s)	Variation		Quality		Quality	
Cube	0.1	0.8	0.8	50	210	60	0.1486	+11.16%	3	0%	5	0%
Cylinder	0.2	0.8	0.8	50	210	60	0.0675	+13.48%	3	0%	4	0%

# CHAPTER FIVE: CONCLUSIONS AND FUTURE WORK

## 5.1. Conclusions

The aim of this study is to develop an extensive model of the FDM 3D-printing process. The difficulty of developing such model is the presence of enormous number of parameters whether the running conditions, the software issues or external factors. The involved parameters: layer height, wall thickness, bottom/top thickness, infill density, temperature and printing speed, are modeled in order to obtain three important concerns; the dimensional variation, edge quality and surface quality of the FDM printed parts by experimental-based model. To achieve deeper insight into the process, the resulted models are optimized by two different techniques; MOGA and MOPSA.

Obviously, the price of including 6 of printing parameters, which is considered weak number compared to the total parameters of the process, in one model affected the regression significance and fitness negatively. However, the models confirm that not a single parameter is influential on the process, though, the interaction between the parameters is found to be more influencing. For both cases, cubes and cylinders, it is found that the most influential terms on the dimensional variation are the infill density, the interaction between wall thickness and printing speed, and the printing speed, whereas the edge quality depends on the interaction between the infill density and printing speed, the interaction between layer height and infill density and the interaction between layer height and printing speed. The surface quality is primarily influenced by wall thickness, the interaction between layer height and infill density and the interaction between temperature and printing speed. Generally, the infill density, the wall thickness, printing speed, the layer height and their interaction are found to be the most

effecting parameters in the FDM process, while the bottom/top thickness and temperature show low significance in this study.

Furthermore, the MOPSA technique outperformed the MOGA technique in the computational time to investigate the optimal parameters of the model, however, the final solutions obtained of both of them are nearly equal. Unexpectedly, the optimization of the two cases of cubes and cylinders resulted the same optimal parameters except the layer height 0.1 mm and 0.2 mm for the cubes and the cylinders, respectively. The difference between the results of the two cases was expected to be the trade-off between wall thickness and printing speed, though, the layer height dominated. Eventually, the optimal printing parameters in this research scope are wall thickness of 0.8 mm, bottom/top thickness of 0.8 mm, infill density of 50%, temperature of 210 °C, printing speed of 60 mm/s and the compensation of the layer height levels [0.1 0.2].

## **5.2. Future Work**

Satisfactorily, the developed model includes 6 printing parameters, however, further investigation on the constant parameters in the FDM printing process is necessary. In addition, many slicing software contain adaptive approaches in providing variable parameters, for example, variable temperatures and printing speeds during the process. To enhance the regression model, higher factors' levels need to be accounted for in order to explore the non-linearity effects of parameters on the FDM process. In addition, the form tolerance analysis might be needed in order to present deeper insight into the final part surface and edge quality.

Overall, it is clearly apparent that FDM process needs more investigations on final printed parts quality. In order to promote FDM as dependable, sustainable and competitive manufacturing process, investigations on input parameters and various outputs such as production time and cost, mechanical properties and surface topography can be analyzed, modeled and optimized.

## REFERENCES

- [1] A. Roschli *et al.*, “Designing for Big Area Additive Manufacturing,” *Addit. Manuf.*, vol. 25, pp. 275–285, Jan. 2019, doi: 10.1016/j.addma.2018.11.006.
- [2] O. A. Mohamed, S. H. Masood, and J. L. Bhowmik, “Optimization of fused deposition modeling process parameters: a review of current research and future prospects,” *Adv. Manuf.*, vol. 3, no. 1, pp. 42–53, Mar. 2015, doi: 10.1007/s40436-014-0097-7.
- [3] T. D. Ngo, A. Kashani, G. Imbalzano, K. T. Q. Nguyen, and D. Hui, “Additive manufacturing (3D printing): A review of materials, methods, applications and challenges,” *Compos. Part B Eng.*, vol. 143, pp. 172–196, Jun. 2018, doi: 10.1016/j.compositesb.2018.02.012.
- [4] X. Wang, M. Jiang, Z. Zhou, J. Gou, and D. Hui, “3D printing of polymer matrix composites: A review and prospective,” *Compos. Part B Eng.*, vol. 110, pp. 442–458, Feb. 2017, doi: 10.1016/j.compositesb.2016.11.034.
- [5] P. Chennakesava and Y. S. Narayan, “Fused Deposition Modeling - Insights,” p. 7, 2014.
- [6] S. Bakrani Balani, F. Chabert, V. Nassiet, and A. Cantarel, “Influence of printing parameters on the stability of deposited beads in fused filament fabrication of poly(lactic acid),” *Addit. Manuf.*, vol. 25, pp. 112–121, Jan. 2019, doi: 10.1016/j.addma.2018.10.012.
- [7] T. Webbe Kerekes, H. Lim, W. Y. Joe, and G. J. Yun, “Characterization of process–deformation/damage property relationship of fused deposition modeling (FDM) 3D-printed specimens,” *Addit. Manuf.*, vol. 25, pp. 532–544, Jan. 2019, doi: 10.1016/j.addma.2018.11.008.
- [8] A. Alafaghani, A. Qattawi, B. Alrawi, and A. Guzman, “Experimental Optimization of Fused Deposition Modelling Processing Parameters: A Design-for-Manufacturing Approach,” *Procedia Manuf.*, vol. 10, pp. 791–803, 2017, doi: 10.1016/j.promfg.2017.07.079.
- [9] Y. Song, Y. Li, W. Song, K. Yee, K.-Y. Lee, and V. L. Tagarielli, “Measurements of the mechanical response of unidirectional 3D-printed PLA,” *Mater. Des.*, vol. 123, pp. 154–164, Jun. 2017, doi: 10.1016/j.matdes.2017.03.051.
- [10] L. Bottini and A. Boschetto, “Interference fit of material extrusion parts,” *Addit. Manuf.*, vol. 25, pp. 335–346, Jan. 2019, doi: 10.1016/j.addma.2018.11.025.
- [11] W. Oropallo and L. A. Piegler, “Ten challenges in 3D printing,” *Eng. Comput.*, vol. 32, no. 1, pp. 135–148, Jan. 2016, doi: 10.1007/s00366-015-0407-0.
- [12] R. Leal *et al.*, “Additive manufacturing tooling for the automotive industry,” *Int. J. Adv. Manuf. Technol.*, vol. 92, no. 5–8, pp. 1671–1676, Sep. 2017, doi: 10.1007/s00170-017-0239-8.
- [13] V. Queral, E. Rincón, V. Mirones, L. Rios, and S. Cabrera, “Dimensional accuracy of additively manufactured structures for modular coil windings of stellarators,” *Fusion Eng. Des.*, vol. 124, pp. 173–178, Nov. 2017, doi: 10.1016/j.fusengdes.2016.12.014.
- [14] C.-Y. Lee and C.-Y. Liu, “The influence of forced-air cooling on a 3D printed PLA part manufactured by fused filament fabrication,” *Addit. Manuf.*, vol. 25, pp. 196–203, Jan. 2019, doi: 10.1016/j.addma.2018.11.012.

- [15] A. Armillotta, "Simulation of edge quality in fused deposition modeling," *Rapid Prototyp. J.*, vol. 25, no. 3, pp. 541–554, Apr. 2019, doi: 10.1108/RPJ-06-2018-0151.
- [16] MathWorks, *MATLAB*. 2021a. [Online]. Available: <https://www.mathworks.com/products/matlab.html>
- [17] S. Singamneni, A. Roychoudhury, O. Diegel, and B. Huang, "Modeling and evaluation of curved layer fused deposition," *J. Mater. Process. Technol.*, vol. 212, no. 1, pp. 27–35, Jan. 2012, doi: 10.1016/j.jmatprotec.2011.08.001.
- [18] C.-C. Kuo *et al.*, "Preparation of starch/acrylonitrile-butadiene-styrene copolymers (ABS) biomass alloys and their feasible evaluation for 3D printing applications," *Compos. Part B Eng.*, vol. 86, pp. 36–39, Feb. 2016, doi: 10.1016/j.compositesb.2015.10.005.
- [19] P. Parandoush and D. Lin, "A review on additive manufacturing of polymer-fiber composites," *Compos. Struct.*, vol. 182, pp. 36–53, Dec. 2017, doi: 10.1016/j.compstruct.2017.08.088.
- [20] A. K. Sood, R. K. Ohdar, and S. S. Mahapatra, "Parametric appraisal of mechanical property of fused deposition modelling processed parts," *Mater. Des.*, vol. 31, no. 1, pp. 287–295, Jan. 2010, doi: 10.1016/j.matdes.2009.06.016.
- [21] D. Hernandez, "Factors Affecting Dimensional Precision of Consumer 3D Printing," *Int. J. Aviat. Aeronaut. Aerosp.*, 2015, doi: 10.15394/ijaaa.2015.1085.
- [22] Stephen Oluwashola Akande and Newcastle University, UK, "Dimensional Accuracy and Surface Finish Optimization of Fused Deposition Modelling Parts using Desirability Function Analysis," *Int. J. Eng. Res.*, vol. V4, no. 04, Apr. 2015, doi: 10.17577/IJERTV4IS040393.
- [23] A. Boschetto and L. Bottini, "Accuracy prediction in fused deposition modeling," *Int. J. Adv. Manuf. Technol.*, vol. 73, no. 5–8, pp. 913–928, Jul. 2014, doi: 10.1007/s00170-014-5886-4.
- [24] B. H. Lee, J. Abdullah, and Z. A. Khan, "Optimization of rapid prototyping parameters for production of flexible ABS object," *J. Mater. Process. Technol.*, vol. 169, no. 1, pp. 54–61, Oct. 2005, doi: 10.1016/j.jmatprotec.2005.02.259.
- [25] R. Anitha, S. Arunachalam, and P. Radhakrishnan, "Critical parameters influencing the quality of prototypes in fused deposition modelling," *J. Mater. Process. Technol.*, p. 4, 2001.
- [26] S. R. Rajpurohit and H. K. Dave, "Effect of process parameters on tensile strength of FDM printed PLA part," *Rapid Prototyp. J.*, vol. 24, no. 8, pp. 1317–1324, Nov. 2018, doi: 10.1108/RPJ-06-2017-0134.
- [27] S. H. Masood, "Intelligent rapid prototyping with fused deposition modelling," *Rapid Prototyp. J.*, vol. 2, no. 1, pp. 24–33, Mar. 1996, doi: 10.1108/13552549610109054.
- [28] A. E. Costa, A. Ferreira da Silva, and O. Sousa Carneiro, "A study on extruded filament bonding in fused filament fabrication," *Rapid Prototyp. J.*, vol. 25, no. 3, pp. 555–565, Apr. 2019, doi: 10.1108/RPJ-03-2018-0062.
- [29] P. M. Pandey, K. Thrimurthulu, and N. V. Reddy \*, "Optimal part deposition orientation in FDM by using a multicriteria genetic algorithm," *Int. J. Prod. Res.*, vol. 42, no. 19, pp. 4069–4089, Oct. 2004, doi: 10.1080/00207540410001708470.



- [30] F. Górski, W. Kuczko, and R. Wichniarek, "INFLUENCE OF PROCESS PARAMETERS ON DIMENSIONAL ACCURACY OF PARTS MANUFACTURED USING FUSED DEPOSITION MODELLING TECHNOLOGY," *Adv. Sci. Technol. – Res. J.*, vol. 7, no. 19, pp. 27–35, Sep. 2013, doi: 10.5604/20804075.1062340.
- [31] Z. Moza, K. Kitsakis, J. Kechagias, and N. Mastorakis, "Optimizing Dimensional Accuracy of Fused Filament Fabrication using Taguchi Design," p. 6.
- [32] R. K. Sahu, S. S. Mahapatra, and A. K. Sood, "A Study on Dimensional Accuracy of Fused Deposition Modeling (FDM) Processed Parts using Fuzzy Logic," *J. Manuf. Sci. Prod.*, vol. 13, no. 3, Jan. 2013, doi: 10.1515/jmmsp-2013-0010.
- [33] M. Pérez, G. Medina-Sánchez, A. García-Collado, M. Gupta, and D. Carou, "Surface Quality Enhancement of Fused Deposition Modeling (FDM) Printed Samples Based on the Selection of Critical Printing Parameters," *Materials*, vol. 11, no. 8, p. 1382, Aug. 2018, doi: 10.3390/ma11081382.
- [34] M. M. Hanon, L. Zsidai, and Q. Ma, "Accuracy investigation of 3D printed PLA with various process parameters and different colors," *Mater. Today Proc.*, vol. 42, pp. 3089–3096, 2021, doi: 10.1016/j.matpr.2020.12.1246.
- [35] A. Elkaseer, S. Schneider, and S. G. Scholz, "Experiment-Based Process Modeling and Optimization for High-Quality and Resource-Efficient FFF 3D Printing," *Appl. Sci.*, vol. 10, no. 8, p. 2899, Apr. 2020, doi: 10.3390/app10082899.
- [36] K. Tong, S. Joshi, and E. Amine Lehtihet, "Error compensation for fused deposition modeling (FDM) machine by correcting slice files," *Rapid Prototyp. J.*, vol. 14, no. 1, pp. 4–14, Jan. 2008, doi: 10.1108/13552540810841517.
- [37] *SolidWorks*. Dessult Systems. [Online]. Available: <https://www.solidworks.com/>
- [38] *Ultimaker Cura*. Ultimaker, 2021. [Online]. Available: <https://ultimaker.com/software/ultimaker-cura>
- [39] R. A. Horn and C. R. Johnson, *Matrix analysis*, 23. print. Cambridge: Cambridge Univ. Press, 2010.
- [40] *Minitab*. 2019. [Online]. Available: <https://www.minitab.com/en-us/>

# APPENDIX

## A. Experimental Results of Cube Samples

Run No.	Parameters						Results		
	LH	Wt	BTt	InD	T	V	Dimensional Variation	Edge Quality	Surface Quality
B1	0.1	0.4	0.8	0.25	190	30	0.1282	2	4
B2	0.2	0.4	0.8	0.25	190	30	0.2110	3	3
B3	0.1	1.2	0.8	0.25	190	30	0.3120	3	5
B4	0.2	1.2	0.8	0.25	190	30	0.1878	3	4
B5	0.1	0.4	1.6	0.25	190	30	0.1999	3	4
B6	0.2	0.4	1.6	0.25	190	30	0.1607	3	3
B7	0.1	1.2	1.6	0.25	190	30	0.2726	3	5
B8	0.2	1.2	1.6	0.25	190	30	0.2172	3	4
B9	0.1	0.4	0.8	0.5	190	30	0.1963	3	3
B10	0.2	0.4	0.8	0.5	190	30	0.0948	2	3
B11	0.1	1.2	0.8	0.5	190	30	0.2192	3	4
B12	0.2	1.2	0.8	0.5	190	30	0.2218	3	4
B13	0.1	0.4	1.6	0.5	190	30	0.2063	2	4
B14	0.2	0.4	1.6	0.5	190	30	0.1452	3	2
B15	0.1	1.2	1.6	0.5	190	30	0.3195	3	4
B16	0.2	1.2	1.6	0.5	190	30	0.1945	3	4
B17	0.1	0.4	0.8	0.25	210	30	0.1135	2	3
B18	0.2	0.4	0.8	0.25	210	30	0.1561	3	3
B19	0.1	1.2	0.8	0.25	210	30	0.2209	3	5
B20	0.2	1.2	0.8	0.25	210	30	0.1753	3	4
B21	0.1	0.4	1.6	0.25	210	30	0.2322	2	4
B22	0.2	0.4	1.6	0.25	210	30	0.1212	3	2
B23	0.1	1.2	1.6	0.25	210	30	0.2342	3	3
B24	0.2	1.2	1.6	0.25	210	30	0.2538	3	3
B25	0.1	0.4	0.8	0.5	210	30	0.1415	3	3
B26	0.2	0.4	0.8	0.5	210	30	0.1457	3	2

B27	0.1	1.2	0.8	0.5	210	30	0.1746	2	4
B28	0.2	1.2	0.8	0.5	210	30	0.1752	3	3
B29	0.1	0.4	1.6	0.5	210	30	0.1512	2	3
B30	0.2	0.4	1.6	0.5	210	30	0.0923	2	3
B31	0.1	1.2	1.6	0.5	210	30	0.1922	3	4
B32	0.2	1.2	1.6	0.5	210	30	0.1190	3	3
B33	0.1	0.4	0.8	0.25	190	60	0.1766	0	3
B34	0.2	0.4	0.8	0.25	190	60	0.1029	3	3
B35	0.1	1.2	0.8	0.25	190	60	0.2902	2	3
B36	0.2	1.2	0.8	0.25	190	60	0.1215	3	5
B37	0.1	0.4	1.6	0.25	190	60	0.2354	2	2
B38	0.2	0.4	1.6	0.25	190	60	0.1845	3	2
B39	0.1	1.2	1.6	0.25	190	60	0.2216	3	4
B40	0.2	1.2	1.6	0.25	190	60	0.1047	3	4
B41	0.1	0.4	0.8	0.5	190	60	0.1156	3	3
B42	0.2	0.4	0.8	0.5	190	60	0.0635	3	2
B43	0.1	1.2	0.8	0.5	190	60	0.0538	3	3
B44	0.2	1.2	0.8	0.5	190	60	0.1252	3	2
B45	0.1	0.4	1.6	0.5	190	60	0.0785	3	4
B46	0.2	0.4	1.6	0.5	190	60	0.1215	3	2
B47	0.1	1.2	1.6	0.5	190	60	0.0457	3	2
B48	0.2	1.2	1.6	0.5	190	60	0.0836	2	2
B49	0.1	0.4	0.8	0.25	210	60	0.1842	2	3
B50	0.2	0.4	0.8	0.25	210	60	0.1380	3	3
B51	0.1	1.2	0.8	0.25	210	60	0.0231	2	3
B52	0.2	1.2	0.8	0.25	210	60	0.1415	2	4
B53	0.1	0.4	1.6	0.25	210	60	0.1348	2	3
B54	0.2	0.4	1.6	0.25	210	60	0.1781	2	3
B55	0.1	1.2	1.6	0.25	210	60	0.1048	2	4
B56	0.2	1.2	1.6	0.25	210	60	0.1496	2	4
B57	0.1	0.4	0.8	0.5	210	60	0.1036	3	3
B58	0.2	0.4	0.8	0.5	210	60	0.0545	3	2
B59	0.1	1.2	0.8	0.5	210	60	0.1356	3	4
B60	0.2	1.2	0.8	0.5	210	60	0.0651	3	4

B61	0.1	0.4	1.6	0.5	210	60	0.1154	2	3
B62	0.2	0.4	1.6	0.5	210	60	0.0622	2	2
B63	0.1	1.2	1.6	0.5	210	60	0.0588	3	4
B64	0.2	1.2	1.6	0.5	210	60	0.1130	2	3

## B. Experimental Results of Cylinder Samples

Run No.	Parameters						Results		
	LH	Wt	BTt	InD	T	V	Dimensional Variation	Edge Quality	Surface Quality
B1	0.1	0.4	0.8	0.25	190	30	0.1282	2	4
B2	0.2	0.4	0.8	0.25	190	30	0.2110	3	3
B3	0.1	1.2	0.8	0.25	190	30	0.3120	3	5
B4	0.2	1.2	0.8	0.25	190	30	0.1878	3	4
B5	0.1	0.4	1.6	0.25	190	30	0.1999	3	4
B6	0.2	0.4	1.6	0.25	190	30	0.1607	3	3
B7	0.1	1.2	1.6	0.25	190	30	0.2726	3	5
B8	0.2	1.2	1.6	0.25	190	30	0.2172	3	4
B9	0.1	0.4	0.8	0.5	190	30	0.1963	3	3
B10	0.2	0.4	0.8	0.5	190	30	0.0948	2	3
B11	0.1	1.2	0.8	0.5	190	30	0.2192	3	4
B12	0.2	1.2	0.8	0.5	190	30	0.2218	3	4
B13	0.1	0.4	1.6	0.5	190	30	0.2063	2	4
B14	0.2	0.4	1.6	0.5	190	30	0.1452	3	2
B15	0.1	1.2	1.6	0.5	190	30	0.3195	3	4
B16	0.2	1.2	1.6	0.5	190	30	0.1945	3	4
B17	0.1	0.4	0.8	0.25	210	30	0.1135	2	3
B18	0.2	0.4	0.8	0.25	210	30	0.1561	3	3
B19	0.1	1.2	0.8	0.25	210	30	0.2209	3	5
B20	0.2	1.2	0.8	0.25	210	30	0.1753	3	4
B21	0.1	0.4	1.6	0.25	210	30	0.2322	2	4
B22	0.2	0.4	1.6	0.25	210	30	0.1212	3	2
B23	0.1	1.2	1.6	0.25	210	30	0.2342	3	3
B24	0.2	1.2	1.6	0.25	210	30	0.2538	3	3

B25	0.1	0.4	0.8	0.5	210	30	0.1415	3	3
B26	0.2	0.4	0.8	0.5	210	30	0.1457	3	2
B27	0.1	1.2	0.8	0.5	210	30	0.1746	2	4
B28	0.2	1.2	0.8	0.5	210	30	0.1752	3	3
B29	0.1	0.4	1.6	0.5	210	30	0.1512	2	3
B30	0.2	0.4	1.6	0.5	210	30	0.0923	2	3
B31	0.1	1.2	1.6	0.5	210	30	0.1922	3	4
B32	0.2	1.2	1.6	0.5	210	30	0.1190	3	3
B33	0.1	0.4	0.8	0.25	190	60	0.1766	0	3
B34	0.2	0.4	0.8	0.25	190	60	0.1029	3	3
B35	0.1	1.2	0.8	0.25	190	60	0.2902	2	3
B36	0.2	1.2	0.8	0.25	190	60	0.1215	3	5
B37	0.1	0.4	1.6	0.25	190	60	0.2354	2	2
B38	0.2	0.4	1.6	0.25	190	60	0.1845	3	2
B39	0.1	1.2	1.6	0.25	190	60	0.2216	3	4
B40	0.2	1.2	1.6	0.25	190	60	0.1047	3	4
B41	0.1	0.4	0.8	0.5	190	60	0.1156	3	3
B42	0.2	0.4	0.8	0.5	190	60	0.0635	3	2
B43	0.1	1.2	0.8	0.5	190	60	0.0538	3	3
B44	0.2	1.2	0.8	0.5	190	60	0.1252	3	2
B45	0.1	0.4	1.6	0.5	190	60	0.0785	3	4
B46	0.2	0.4	1.6	0.5	190	60	0.1215	3	2
B47	0.1	1.2	1.6	0.5	190	60	0.0457	3	2
B48	0.2	1.2	1.6	0.5	190	60	0.0836	2	2
B49	0.1	0.4	0.8	0.25	210	60	0.1842	2	3
B50	0.2	0.4	0.8	0.25	210	60	0.1380	3	3
B51	0.1	1.2	0.8	0.25	210	60	0.0231	2	3
B52	0.2	1.2	0.8	0.25	210	60	0.1415	2	4
B53	0.1	0.4	1.6	0.25	210	60	0.1348	2	3
B54	0.2	0.4	1.6	0.25	210	60	0.1781	2	3
B55	0.1	1.2	1.6	0.25	210	60	0.1048	2	4
B56	0.2	1.2	1.6	0.25	210	60	0.1496	2	4
B57	0.1	0.4	0.8	0.5	210	60	0.1036	3	3
B58	0.2	0.4	0.8	0.5	210	60	0.0545	3	2

<b>B59</b>	0.1	1.2	0.8	0.5	210	60	0.1356	3	4
<b>B60</b>	0.2	1.2	0.8	0.5	210	60	0.0651	3	4
<b>B61</b>	0.1	0.4	1.6	0.5	210	60	0.1154	2	3
<b>B62</b>	0.2	0.4	1.6	0.5	210	60	0.0622	2	2
<b>B63</b>	0.1	1.2	1.6	0.5	210	60	0.0588	3	4
<b>B64</b>	0.2	1.2	1.6	0.5	210	60	0.1130	2	3